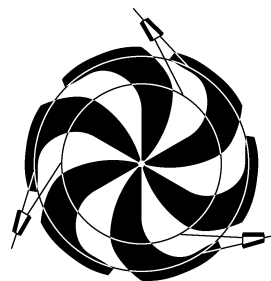


TRIUMF



ANNUAL REPORT SCIENTIFIC ACTIVITIES 2003

ISSN 1492-417X

**CANADA'S NATIONAL LABORATORY
FOR PARTICLE AND NUCLEAR PHYSICS**

OPERATED AS A JOINT VENTURE

MEMBERS:

THE UNIVERSITY OF ALBERTA
THE UNIVERSITY OF BRITISH COLUMBIA
CARLETON UNIVERSITY
SIMON FRASER UNIVERSITY
THE UNIVERSITY OF VICTORIA

ASSOCIATE MEMBERS:

THE UNIVERSITY OF GUELPH
THE UNIVERSITY OF MANITOBA
McMASTER UNIVERSITY
L'UNIVERSITÉ DE MONTRÉAL
QUEEN'S UNIVERSITY
THE UNIVERSITY OF REGINA
THE UNIVERSITY OF TORONTO

UNDER A CONTRIBUTION FROM THE
NATIONAL RESEARCH COUNCIL OF CANADA

DECEMBER 2004

The contributions on individual experiments in this report are outlines intended to demonstrate the extent of scientific activity at TRIUMF during the past year. The outlines are not publications and often contain preliminary results not intended, or not yet ready, for publication. Material from these reports should not be reproduced or quoted without permission from the authors.

Experiment 768**Generalized FFLO state and anomaly of flux line lattice state in novel superconductors***(R. Kadono, J. Akimitsu, KEK-IMSS, Aoyama-Gakuin)*

While the original goal of this proposal was to elucidate the anomalous magnetic response of quasiparticle excitation in CeRu₂ and related compounds, we have been looking for typical type II superconductors which could be compared with CeRu₂ as standard references. In 2003 we continued our search for such compounds including those which were newly discovered. Recently, a new ternary silicide, Sr(Ga,Si)₂, which has the AlB₂-type structure similar to that of MgB₂, was reported to be a superconductor with $T_c = 3.4$ K, stimulating active investigation of analogous compounds. In this class of materials, ternary silicide Ca(Al_{0.5}Si_{0.5})₂ has the highest critical temperature $T_c = 7.7$ K [Imai *et al.*, Appl. Phys. Lett. **80**, 1019 (2002)]. It is reported on this compound that the behaviour of electron-heat capacity deviates from that of the BCS-type, and that the effect of hydrostatic pressure on T_c is positive. Unfortunately, despite various experiments so far, there is very little known on the structure of superconducting order parameter in this compound. In order to obtain a clue in this matter, we measured magnetic penetration depth (λ) vs. temperature and field in a polycrystalline Ca(Al_{0.5}Si_{0.5})₂. The μ SR experiments were performed on the M1 5 beam line using the HiTime spectrometer. The specimen, having a dimension of about 7×7 mm², was mounted on the sample holder of a cryostat and then field-cooled at every magnetic field point to minimize the effect of flux pinning. The temperature (T) and field (H) dependence of transverse field (TF)- μ SR spectrum was obtained at $H = 2.0$ T and $T = 2.0$ K, respectively. It is well established that the Gaussian relaxation rate σ measured by TF- μ SR is predominantly determined by λ , and thus by the superconductive carrier density n_s in the following relation

$$\sigma^{-1} \propto \lambda^2 = \frac{m^* c^2}{4\pi n_s e^2}.$$

This equation indicates that λ is enhanced upon the reduction of n_s due to the quasiparticle excitation. For the ideal triangular flux line lattice (FLL) with isotropic effective carrier mass m^* , λ is given by the following relation

$$\sigma[\mu s^{-1}] = 4.83 \times 10^4 (1-h)[1+3.9(1-h)^2]^{1/2} \lambda^{-2} [\text{nm}],$$

where $h = H/H_{c2}$ with H_{c2} being the upper critical field. Therefore, provided that H_{c2} is known, one can deduce λ from σ at arbitrary field. The T dependence

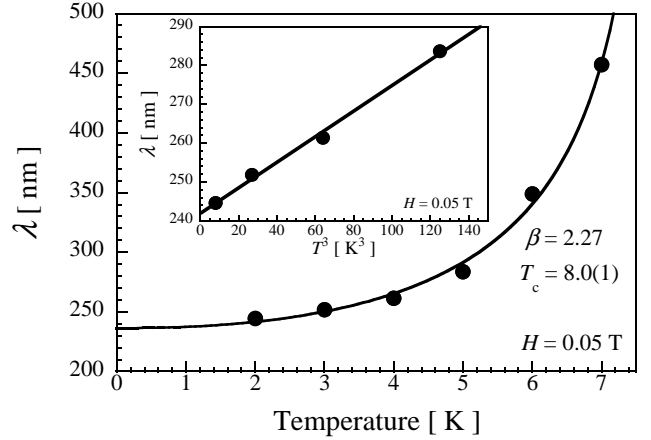


Fig. 106. Temperature dependence of the magnetic penetration depth λ at 0.05 T. The inset shows the λ plotted against T^3 . The solid line is a fitting result with $\lambda(t) = \lambda(0)/\sqrt{1-t^\beta}$.

of λ obtained from the analysis using a Gaussian model is shown in Fig. 106. Over the region below $T_c \sim 7.7$ K where the FLL is formed, λ increases with decreasing temperature. According to the empirical two-fluid model (which is a good approximation of the BCS theory), the following relation is expected to hold

$$\lambda(t) = \lambda(0) \frac{1}{\sqrt{1-t^4}},$$

where $t = T/T_c$. The solid line is the result of fitting analysis by a similar formula with an arbitrary power

$$\lambda(t) = \lambda(0) \frac{1}{\sqrt{1-t^\beta}}.$$

When both β and T_c are assumed to be free parameters, the above equation yields a good agreement with data for $\beta = 2.27$ and $T_c = 8.0(1)$ K. The result also means that the deviation of λ ,

$$\Delta\lambda = \lambda(t) - \lambda(0),$$

exhibits a tendency predicted for the case of line nodes (d -wave pairing) with some disorder (i.e. dirty limit, where $\Delta\lambda \propto T^2$). Compared with the case of isotropic gap ($\Delta_k = \Delta_0$), the quasiparticle excitations are enhanced along nodes ($|\Delta_k| = 0$) to reduce average n_s , leading to the enhancement of λ . As shown in the inset of Fig. 106, λ at low temperature behaves linearly against T^3 , suggesting that the order parameter in Ca(Al_{0.5}Si_{0.5})₂ has a large anisotropy. This is further supported by the magnetic field dependence of λ . As shown in Fig. 107, λ clearly exhibits a strong field dependence, where λ increases almost linearly with h . This is similar to the cases of NbSe₂, YNi₂B₂C, and

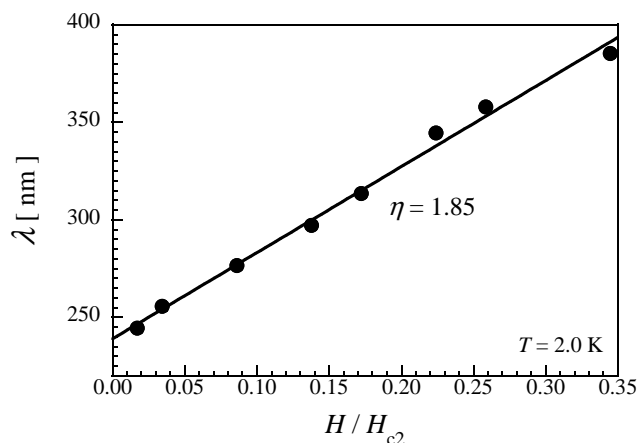


Fig. 107. Magnetic field dependence of the penetration depth λ at 2.0 K. The solid line is a fitting result with $\lambda(h)/\lambda(0) = 1 + \eta h$.

MgB₂, where such T/H -dependence of λ was observed; by now, there is ample evidence that they all have some anisotropy (including double gap) in the order parameter. The solid line is the result of fitting by the following linear relation

$$\frac{\lambda(h)}{\lambda(0)} = 1 + \eta h,$$

where η is a dimension-less parameter which represents the strength of the pair breaking effect. Fitting yields $\eta = 1.85$ (with $\lambda(0) = 239.05$ nm, $H_{c2} = 3.0$ T at 2 K) which is comparable with that in NbSe₂, YNi₂B₂C and MgB₂ (i.e. $\eta = 1.61, 0.97$, and 1.27 , respectively). Unfortunately, our results were obtained using a polycrystalline sample, which makes it difficult to deduce λ by analyzing data using the well-defined microscopic model.

Early experiments on high quality single crystal samples of Ca(Al_{0.5}Si_{0.5})₂ have reported that the upper critical field has an anomalous angular dependence which deviates from the Ginsburg-Landau anisotropic mass model. Moreover, very recent reports suggest that the crystal structure has clear five-fold and two-fold superlattice. Therefore, we are preparing high quality single crystals of Ca(Al_{0.5}Si_{0.5})₂ for further μ SR study of this compound in more detail.

Experiment 842

Mu-substituted free radicals in sub- and super-critical water

(P.W. Percival, SFU)

There is currently great interest in organic reactions in superheated water, and research in this area is motivated by a surprising diversity of applications: geochemical production of petroleum, biology in hydrothermal vents, corrosion in steam generators, destruction of hazardous waste, and the development

of environmentally benign chemical processes. However, progress on many of these fronts is hampered by lack of detailed knowledge of the kinetics and mechanisms of chemical reactions under hydrothermal conditions. Most studies to date have relied on end-product analysis and modelling to infer multi-step reaction sequences. Ideally, reaction intermediates should be studied in real time *in situ*. In practice most techniques are limited by the technical demands of the harsh environment – water is a corrosive solvent at high pressure and high temperature (hydrothermal chemistry is important up to and through the critical point of water, at 374°C, 220 bar). The study of free radicals is particularly difficult under such conditions.

Experiment 842 was designed to study free radicals in hydrothermal systems by using the positive muon as a spin probe. Since a positive muon can act as the nucleus of the hydrogen-like atom, muonium (Mu), it can be used to study H atom reactions and free radicals incorporating H. We were quickly able to demonstrate the feasibility of such studies by using transverse-field μ SR to detect muoniated free radicals over a wide range of conditions, all the way to supercritical [Percival *et al.*, Phys. Chem. Chem. Phys. **2**, 4717 (2000)]. However, unambiguous identification of free radicals requires knowledge of proton (or other nuclear) hyperfine constants, in addition to the muon hyperfine constant obtained by μ SR. In principle these hyperfine data can be obtained by muon avoided level-crossing resonance, and indeed we have done so in other projects, using the HELIOS spectrometer (see for example the report on Expt. 883). Unfortunately our high pressure cell was incompatible with HELIOS, which is based on a warm bore superconducting magnet with limited access, in contrast to the relatively open geometry of the SFUMU spectrometer used in previous high pressure experiments. Thus the project was stalled until the fall when a prototype high-pressure/high-temperature cell was built to fit HELIOS.

The new cell was a success, and immediately provided valuable new data. Since high momentum muons are required to penetrate the window of the pressure cell, Expt. 842 has to use beam line M9B, which does not have the spin rotation feature of M15 and M20. Thus it was expected that the longitudinal field installation of HELIOS would preclude standard transverse-field μ SR experiments. Surprisingly it was found that M9B has a significant transverse component of muon spin polarization, so that both μ SR and μ LCR experiments were possible in the same installation, with an appropriate adjustment of the positron counter positions.

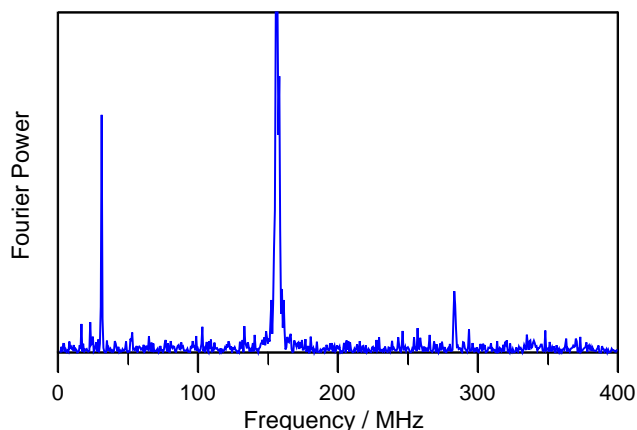


Fig. 108. μ SR spectrum of the *tert*-butyl radical in water at 300°C and 245 bar.

The transverse polarization on M9B has yet to be investigated systematically, but its utility is clearly demonstrated by the excellent spectrum evident in Fig. 108. The sample used for this spectrum was a solution of *tert*-butanol in water, which undergoes reaction in superheated water to form isobutene, $(\text{CH}_3)_2\text{C}=\text{CH}_2$. The reaction of muonium with isobutene results in the muoniated *tert*-butyl radical. The assignment of the *tert*-butyl radical structure, $(\text{CH}_3)_2\dot{\text{C}}\text{CH}_2\text{Mu}$, was originally based on the magnitude of the muon hyperfine coupling only. However, with the new cell it was possible to also collect μ LCR spectra. One example is shown in Fig. 109. There are two resonances apparent (two overlapping differential line shapes), as expected for the slightly different proton coupling constants for the CH_3 and CH_2Mu groups.

There was never much doubt about the identity of the *tert*-butyl radical formed in hot aqueous solutions of *tert*-butanol, hence its use as a test case. In contrast, the detection of more than one radical in superheated aqueous solutions of acetone presented a novel problem

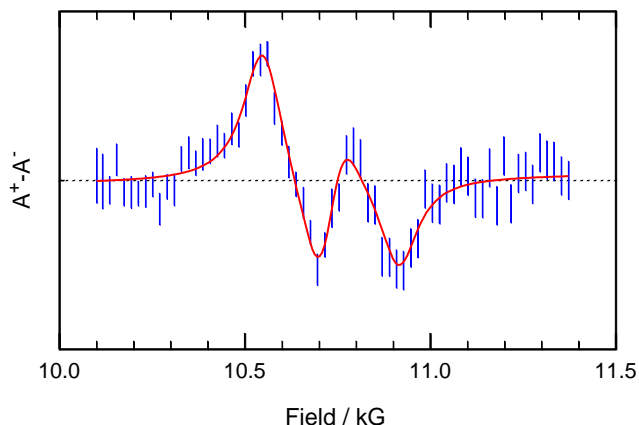


Fig. 109. μ LCR spectrum of the *tert*-butyl radical in water at 200°C and 250 bar.

of great interest to organic chemists. At low temperatures Mu adds to the ketone group of acetone, to form the radical $(\text{CH}_3)_2\dot{\text{C}}\text{OMu}$ (structure II in Fig. 110). On the strength of μ SR spectra alone, we suggested [Ghandi *et al.*, J. Am. Chem. Soc. **125**, 9594 (2003)] that at high temperature the keto form of acetone is in equilibrium with the isomeric enol form, which is more reactive by virtue of the $\text{C}=\text{C}$ double bond. Under these conditions reaction of muonium should result in the radical $\text{CH}_3\dot{\text{C}}(\text{OH})\text{CH}_2\text{Mu}$ (structure I), as indicated in the reaction scheme of Fig. 110. The μ LCR spectrum shown in Fig. 111 confirms this. Once again one sees the effect of two overlapping resonances, in this case even closer together than for the spectrum in Fig. 109.

Further studies should allow us to quantify the temperature dependence of the keto-enol equilibrium as well as the molecular dynamics of the radical products. It is important to realise that muonium is being used here as a passive probe of the keto-enol equilibrium, and that no other spectroscopic technique has ever been applied to probe this phenomenon under such extreme conditions. In fact literature data extends only up to 54°C!

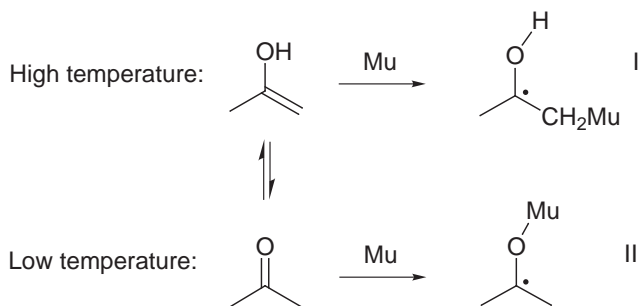


Fig. 110. Muonium addition to the enol and keto forms of acetone in water (upper and lower reactions, respectively).

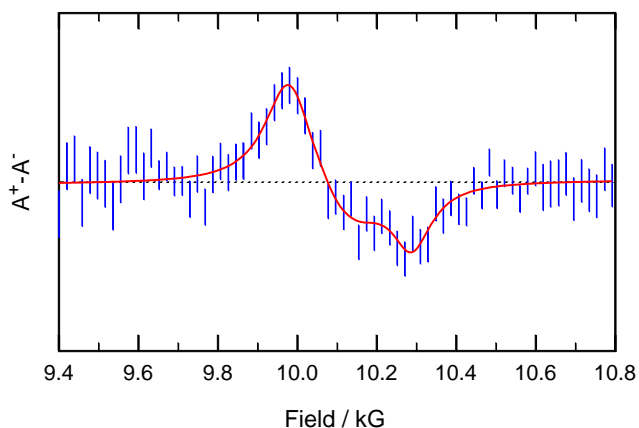


Fig. 111. μ LCR spectrum of the muoniated radical detected in an aqueous solution of acetone in water at 350°C and 250 bar.

Experiment 847

Electron-doped high- T_c superconductors

(J.E. Sonier, F.D. Callaghan, SFU)

Introduction

Our recent research on electron-doped high- T_c superconductors $R_{2-x}\text{Ce}_x\text{CuO}_4$ ($R = \text{La, Pr, Nd, Sm}$ or Eu) has been facilitated by progress in the growth of high quality single crystals of these materials. The issue of sample quality is one reason for the relatively slow advancement in our understanding of the electron-doped materials when compared with the more widely studied hole-doped superconductors. Another reason is the presence of both copper and rare earth magnetic moments. This makes it more difficult to isolate the contribution of the vortex lattice to the measured internal magnetic field distribution.

$\text{Pr}_{2-x}\text{Ce}_x\text{CuO}_4$ (PCCO)

In PCCO at a relatively low magnetic field strength (91 Oe), we observed an increase in local magnetic field at the muon stopping site below the superconducting transition temperature, T_c . Dipolar field calculations have allowed us to ascribe this to magnetic field-induced antiferromagnetic ordering of the Cu spins throughout the volume of the sample. The calculations show that the induced field at the muon site is due to a canting of the Cu spins out of the a-b plane by about 12° . The details of this work appear in a recent publication [Sonier *et al.*, Phys. Rev. Lett. **91**, 147002 (2003)].

$\text{Nd}_{2-x}\text{Ce}_x\text{CuO}_4$ (NCCO)

Most of our work in the last year has concentrated on NCCO. Whereas the ground state of the Pr^{3+} ions in PCCO is non-magnetic, the Nd^{3+} ions in NCCO have a relatively large magnetic moment – approximately $0.5 \mu_B/\text{ion}$ at 5 K in the parent compound Nd_2CuO_4 , which is reduced slightly in Ce-doped crystals due to a reduction in the magnitude of the Cu-Nd exchange field at the Nd site.

In order to induce superconductivity, it is necessary to lower the oxygen content by subjecting the Ce-doped samples to a severe annealing process. We studied a single crystal of NCCO in both the as-grown (pre-annealing) and superconducting (post-annealing) phases. The annealed crystal had a relatively sharp transition to the superconducting state at 23 K, which is indicative of a high quality, near optimally doped sample.

Zero-field μSR (ZF- μSR) measurements showed the magnetism of the as-grown and superconducting samples to be very similar down to temperatures of approximately 10 K, below which a marked difference emerged. Figure 112 shows the time-evolution of the muon spin polarization in each sample at $T = 2.75$ K.

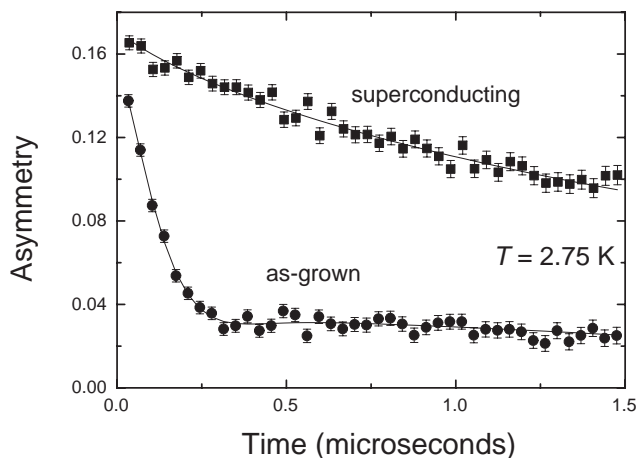


Fig. 112. Zero-field time-evolution of the muon spin polarization at $T = 2.75$ K in both the as-grown and superconducting phases of NCCO.

It can be seen that the muon spin polarization decays much more rapidly in the as-grown sample. In addition, the time-spectrum for the as-grown sample is best fit with a component oscillating at approximately 1 MHz, which is indicative of static magnetic order. The oscillating component first appears around $T = 6$ K and our analysis shows that by 2.6 K 80% of the sample is magnetically ordered. Based on a comparison with neutron and X-ray magnetic scattering experiments on the parent compound Nd_2CuO_4 , we postulate that the most likely source of such widespread order in the as-grown sample is antiferromagnetic ordering of the Nd^{3+} spins. It is known that both Ce-doping and annealing cause a reduction of the Néel temperature for Cu in these materials. This explains why we don't see Cu magnetic order in either the as-grown or superconducting samples. An interesting result is that Nd ordering is not observed in the annealed sample, which implies that Ce-doping has caused a reduction of the Nd ordering temperature. This is due to a suppression of the Cu moment in the annealed sample, which in turn lowers the induced moment on the Nd^{3+} ions due to the Cu-Nd exchange field. These results highlight the role of the Cu-Nd coupling in the ordering of the Nd^{3+} spins in current-generation single crystals.

Transverse-field μSR (TF- μSR) experiments were also performed. TF- μSR measurements at $H = 5$ kOe and parallel to the c axis of the crystal show a large negative μ^+ Knight shift, due primarily to the paramagnetic Nd^{3+} moments (see Fig. 113). The μ^+ Knight shift is a measure of the local magnetic susceptibility which is inaccessible to bulk probes as such measurements are dominated by the diamagnetic response of the superconductor below T_c .

The Nd^{3+} moments contribute a broad Gaussian component to the internal magnetic field distribution

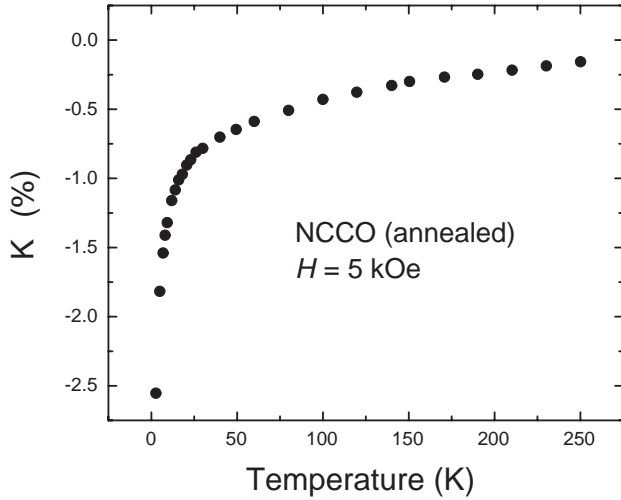


Fig. 113. μ^+ Knight shift in superconducting NCCO at $H = 5$ kOe.

in the vortex state. However, the high quality of the sample we studied allowed us to distinguish the asymmetric lineshape of the vortex lattice for the first time in this material. This means that the contributions from the vortex lattice and the electronic magnetic moments can now be separated, which is crucial for accurate measurements of the magnetic penetration depth and the vortex core size. An extensive analysis is currently under way to determine the temperature dependence of these quantities.

An example of such a lineshape can be seen in Fig. 114. The data were acquired at $T = 2.75$ K in a transverse magnetic field of 5 kOe directed perpendicular to the CuO_2 planes. The data are best fit assuming a square vortex lattice, in agreement with recent neutron scattering results. The pronounced shoulder in the lineshape at around 65.3 MHz is characteristic of a square vortex lattice.

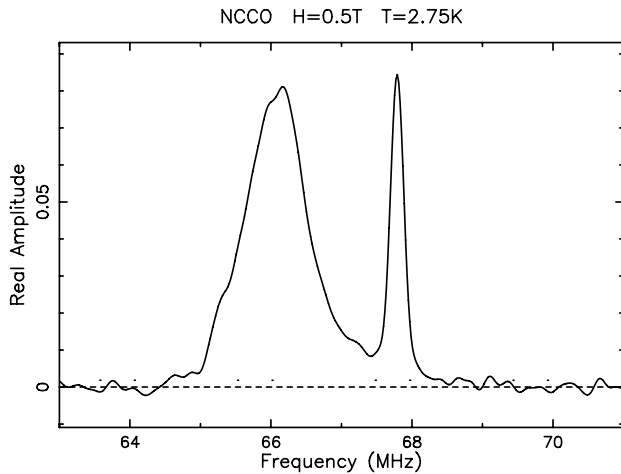


Fig. 114. Fast Fourier transform of the muon spin depolarization time-spectrum in the vortex state of NCCO. Note the characteristic asymmetric lineshape of the vortex lattice in a type-II superconductor.

Experiment 851

μ^+ SR in ruthenate and cuprate superconductors

(D.R. Harshman, Physikon Research Corp.)

The pairing state symmetry of $\text{YBa}_2\text{Cu}_3\text{O}_7$

Last year, we reported on our work [Harshman *et al.*, Int. J. Mod. Phys. **B17**, 3582 (2003); *ibid.*, Phys. Rev. B (in press); *ibid.*, SEMHTS Conf., Miami, FL] showing that the true character of the ground-state symmetry of $\text{YBa}_2\text{Cu}_3\text{O}_7$ is best described by the two-fluid model. We came to this conclusion by using a self-consistent model that incorporated temperature-activated de-pinning of the fluxons, which can mask the underlying order parameter. We showed that others had misinterpreted this pinning behaviour as evidence for d -wave pairing, and estimated that the probability that the non-local d -wave model [Amin *et al.*, Phys. Rev. Lett. **84**, 5864 (2000)] gives a better fit than the two-fluid model is less than 4×10^{-6} (best χ^2 per degree of freedom = 2.38 for two-fluid, compared to 13 for non-local d -wave).

We have continued our studies of single-crystal $\text{YBa}_2\text{Cu}_3\text{O}_7$, looking more closely at the character of the pinning. Recent transverse-field data acquired at 250 Oe show no evidence of a linear component, with the effective penetration depth exhibiting a flat temperature dependence as $T \rightarrow 0$ as is expected for s -wave superconductivity. The Fourier transform of data taken at 3 K is given in Fig. 115, and shows the familiar asymmetric lineshape associated with the formation of a vortex lattice. Little evidence of temperature-activated de-pinning is evident at this field, consistent with a strongly pinned vortex lattice. To show that the vortex lattice is, indeed, strongly pinned, we cooled the

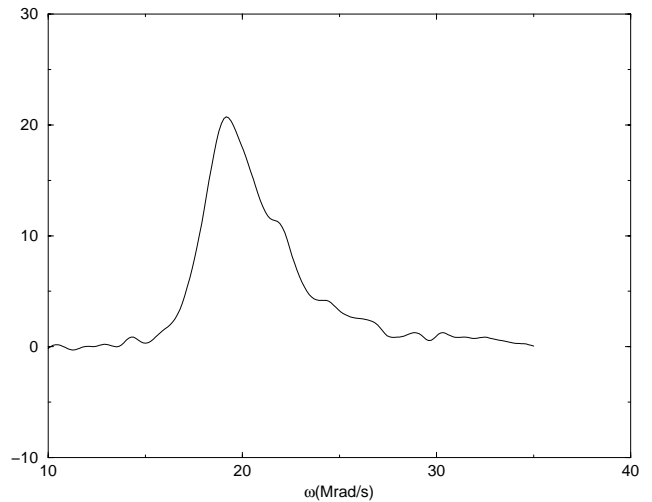


Fig. 115. Fourier transform of data taken at 3 K in 250 Oe.

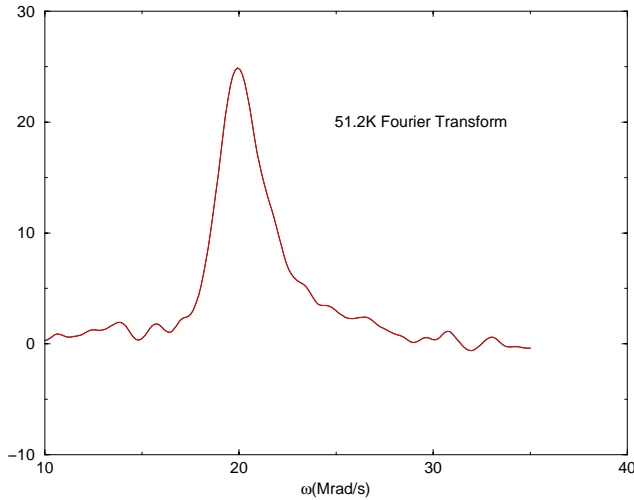


Fig. 116. Fourier transform of data taken at 51.2 K in 0 Oe.

sample in field to low temperatures, turned the field off, and acquired zero-field data at various elevated temperatures. The Fourier transform of data taken at 51.2 K is shown in Fig. 116. The characteristic shape reflecting the presence of a persisting vortex lattice is clearly evident, indicating that the fluxons are still pinned.

This result corroborates our assertion that strong pinning, which was earlier found to be present in powders [Harshman *et al.*, Phys. Rev. **B36**, 2386 (1987)] and early (heavily twinned) crystals [Harshman *et al.*, Phys. Rev. **B39**, 851 (1989)], suppresses the effects of temperature-activated de-pinning. It is only after the $\text{YBa}_2\text{Cu}_3\text{O}_7$ crystal quality improved that the effects of temperature-activated de-pinning, already observed in single-crystal $\text{Bi}_2\text{Sr}_2\text{CaCu}_2\text{O}_8$ [Harshman *et al.*, Phys. Rev. Lett. **67**, 3152 (1991)] became evident, masking the true *s*-wave character of the pairing state.

Experiment 852

Magnetic phases in geometrically frustrated rare earth pyrochlores

(S. Dunsiger, McMaster; R. Kiefl, UBC; J. Gardner, NIST)

Since Anderson considered the problem of antiferromagnetic ordering on the pyrochlore lattice in 1956 [Phys. Rev. **102**, 1008 (1956)], there has been a great deal of interest in systems where the magnetic ions occupy the vertices of edge or corner sharing triangular units [Ramirez, *Magnetic Materials: A Handbook on the Properties of Magnetic Substances and Related Phenomena* (2000)]. In these cases the natural magnetic coupling between ions is said to be geometrically frustrated. The pyrochlore transition metal oxides of general formula $\text{A}_2\text{B}_2\text{O}_7$ are composed of networks of corner-sharing tetrahedra such that it may not be pos-

sible to energetically satisfy all the magnetic interactions simultaneously. The curiosity about these systems stems from the possibility that if conventional magnetic order is highly frustrated then one may find novel low temperature behaviour. There is now considerable evidence that the low temperature state is fragile, i.e. it depends sensitively on a variety of factors such as anisotropy, the range of the spin-spin interactions, thermal and quantum fluctuations and residual disorder.

The purpose of Expt. 852 is to apply μSR to further our understanding of the effect of this frustration on the ground state and low lying magnetic excitations in the pyrochlores, in particular the rare earth titanates $\text{RE}_2\text{Ti}_2\text{O}_7$, where only the A site is magnetic. Recent theoretical efforts have focused on the effect of the dipolar interaction as the leading perturbation, particularly relevant in the study of rare earth systems, which have large dipole moments ($> 1 \mu_B$) and weak exchange interactions. Competing dipolar and superexchange interactions between Ising spins have been studied within the spin-ice type model by Siddharthan *et al.* [Phys. Rev. Lett. **83**, 1854 (1999)] and den Hertog and Gingras [Phys. Rev. Lett. **84**, 3430 (2000)].

$\text{Ho}_2\text{Ti}_2\text{O}_7$: a spin ice

Water ice is made up of oxygen atoms which form a hexagonal lattice (wurtzite structure). Of the 4 hydrogen atoms arranged tetrahedrally around each oxygen atom, two form strong covalent O–H bonds and are close to it to form a water molecule; the remaining two are hydrogen bonded and further removed. The hydrogen ion bonds between atoms form electric dipoles, so they can conveniently be represented by arrows placed on the bonds pointing towards the end occupied by the ion. The ice rule is then equivalent to saying that at each site there are two arrows pointing in and two out, as shown in Fig. 117.

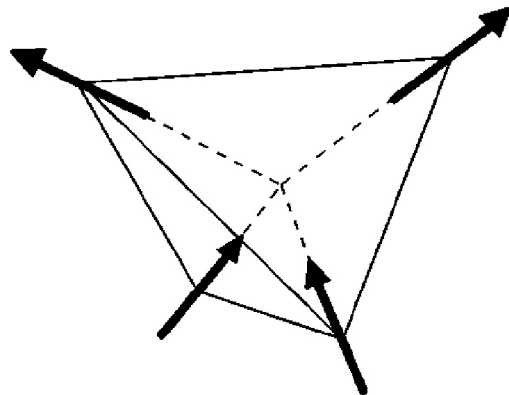


Fig. 117. Ground state configuration of spins on a single tetrahedron given ferromagnetic interactions and strong easy axis anisotropy along the dashed lines.

Spin orientation thus plays a similar role to that of hydrogen position in ice and magnetic analogues of water ice, so called “spin ice”, are currently of much interest [Ramirez *et al.*, Nature **399**, 333 (1999); Harris, Nature **399**, 311 (1999)]. Moessner [Phys. Rev. **B57**, R5587 (1998)] has shown that a strongly anisotropic classical Heisenberg model on the pyrochlore lattice can be mapped onto an Ising pseudospin model with an exchange constant opposite in sign. In the case of strong anisotropy ($|J/D| \ll 1$) the anisotropy term dominates, constraining the spins to lie along the $\langle 111 \rangle$ axes. The exchange term defines the direction in which they point, such that the enclosing angle between any pair may only take on values of 70.5° or 109.5° . Thus, counterintuitively, a system of spins situated on the vertices of corner sharing tetrahedra where the interactions are ferromagnetic may also be geometrically frustrated, provided the spins are constrained by anisotropy to point along the $\langle 111 \rangle$ axes.

Experimentally, the magnetic ions in a number of pyrochlores have recently been found to be subject to significant single ion anisotropies, whose local easy axis is along the $\langle 111 \rangle$ directions and which are thus candidates for spin ice behaviour. To date, the most extensively studied spin ice material is $\text{Ho}_2\text{Ti}_2\text{O}_7$ [Harris *op. cit.*; Harris *et al.*, J. Magn. Magn. Mater. **177-181**, 757 (1998)]. The Ho^{3+} ion is Ising like due to crystal field splittings which result in a ground state doublet with $J_z = \pm 8$ and the next excited state ~ 250 K higher [Siddharthan *et al.*, *op. cit.*]. This suggests that at low temperatures $\text{Ho}_2\text{Ti}_2\text{O}_7$ is well described as a quasi spin 1/2 Ising system. Neutron scattering measurements indicate that no long range order develops down to temperatures of at least 0.35 K in zero magnetic field, but instead, short range ferromagnetic correlations are observed [Harris *et al.*, J. Magn. Magn. Mater. *op. cit.*]. The idea which seems to be emerging is that there is no phase transition, but rather a continuous slowing down of spin fluctuations as the temperature is reduced, due to the development of energy barriers. A number of ordered phases have also been observed on application of a magnetic field, as well as history dependent behaviour. Monte Carlo simulations by Harris *et al.* [Phys. Rev. Lett. **81**, 4496 (1998)] show that the degree of degeneracy breaking depends on the direction of the applied field relative to the crystal axes and this has been confirmed by dc magnetization measurements [Cornelius *et al.*, Phys. Rev. **B64**, 060406 (2001)].

Monte Carlo simulations have been able to describe the magnetic susceptibility and diffuse magnetic neutron scattering results well, but the nature of the spin dynamics below 1 K has only been very briefly studied [Harris *et al.*, J. Magn. Magn. Mater. *op. cit.*] using

μSR . Our group has now completed a lengthy series of $1/T_1$ measurements on the $\langle 100 \rangle$, $\langle 110 \rangle$ and $\langle 111 \rangle$ orientations of $\text{Ho}_2\text{Ti}_2\text{O}_7$ in the dilution refrigerator on M15. In a low longitudinal field (LF) of 0.003 T the μ^+ spin depolarized too quickly to be observed. This is attributed to rapid Ho^{3+} spin fluctuations in the GHz range in the paramagnetic regime.

$\text{Ho}_2\text{Ti}_2\text{O}_7$ ($H \parallel \langle 100 \rangle$, $\langle 110 \rangle$ and $\langle 111 \rangle$)

Typical spectra at a higher field of 2 T applied along the $\langle 100 \rangle$ direction are shown in Fig. 118. At high temperatures of the order of 20 K, a full asymmetry non-exponential muon spin depolarization signal is observed. To account for the non-exponential behaviour, the data have been analyzed assuming a distribution of relaxation rates λ . In general, in low longitudinal field experiments in the “motionally narrowed” limit of rapid spin fluctuations, the muon spin depolarization associated with each magnetically inequivalent site i is well described by a single exponential $\exp(-\lambda t)$. The relaxation rate $\lambda = 2\Delta^2/\nu$, where $\Delta^2/\gamma_\mu^2 = \langle B_i^2 \rangle$ is the second moment of the internal magnetic field B_i ($i = x, y, z$), ν is the mean fluctuation rate for fluctuations in B_i , and γ_μ is the muon gyro-magnetic ratio. For simplicity, a flat distribution of relaxation rates has been assumed between $0 < \lambda < 2\Lambda$. The overall depolarization function then becomes

$$G_Z(t) = \frac{1}{2\Lambda t} [1 - \exp(-2\Lambda t)]. \quad (1)$$

The distribution of relaxation times observed in $\text{Ho}_2\text{Ti}_2\text{O}_7$ is remarkable. In dilute alloys this may be explained by the fact that the muon stops at different distances from the magnetic ion. However, one expects

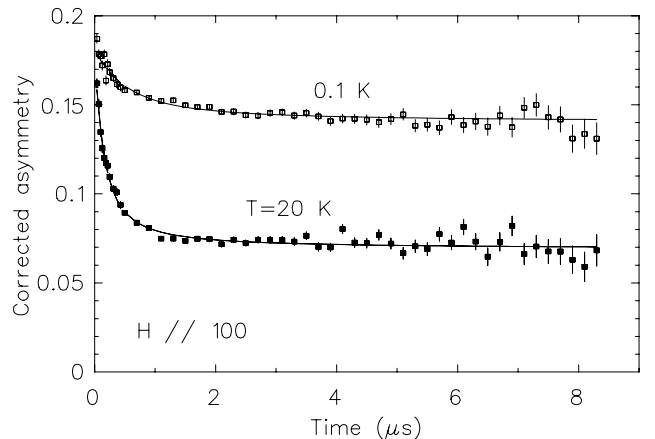


Fig. 118. Typical spectra in $\text{Ho}_2\text{Ti}_2\text{O}_7$ in a longitudinal field of 2 T applied along the $\langle 100 \rangle$ direction. A non-relaxing component due to muons which miss the sample, landing in the silver sample holder, is also present. As the temperature is reduced, an additional non-relaxing signal develops, which is attributed to static internal fields within the sample.

much less variance in a dense system of magnetic ions such as the oxide pyrochlores. This suggests that in this system there are a range of Ho^{3+} spin fluctuation rates.

The results of temperature scans in a longitudinal field of 2 T are summarized in Figs. 119 and 120. Above 5 K the data are well described by Eq. 1. The muon spin relaxation rate decreases with temperature as $\mu_B H/k_B T$ grows and the sample becomes increasingly magnetized. It seems likely that the spin dynamics are being altered as the electronic Zeeman splitting first becomes comparable with, and then exceeds, the exchange coupling \mathcal{J} . However, below 5 K the non-relaxing component develops (see Fig. 118) at the expense of the relaxing component. The amplitudes of

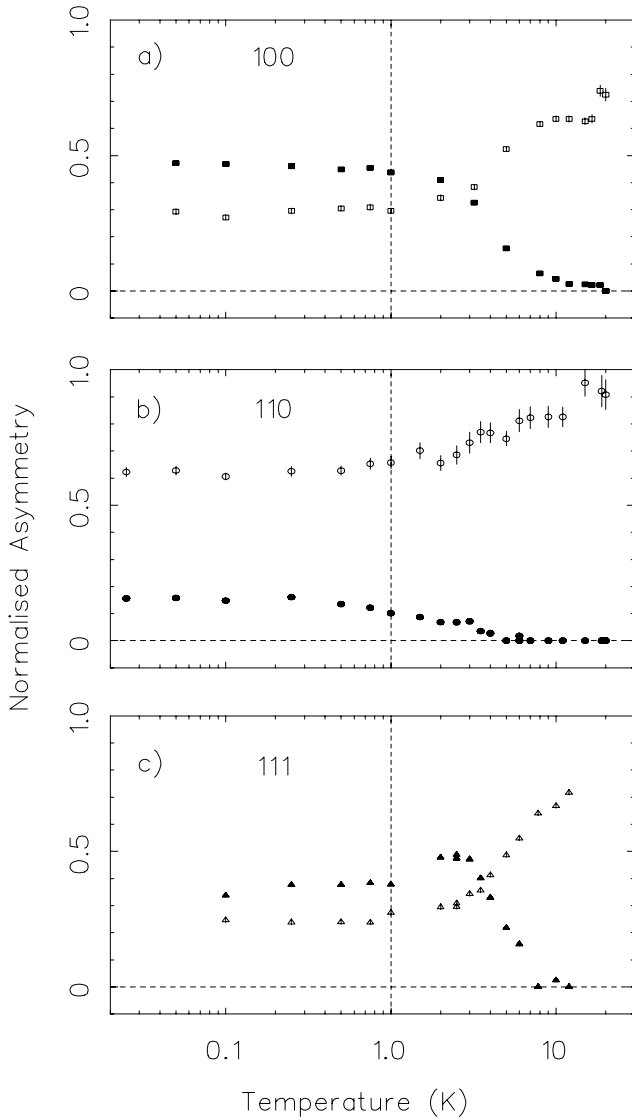


Fig. 119. Two component asymmetry in $\text{Ho}_2\text{Ti}_2\text{O}_7$ as a function of temperature. Magnetic field applied along the a) 100, b) 110 and c) 111 directions. The non-relaxing components are indicated by the filled symbols.

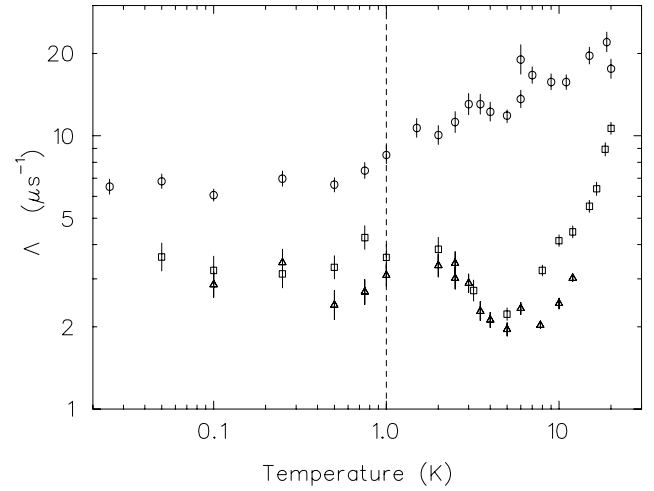


Fig. 120. Characteristic range Λ of relaxation rates of the muon spin polarization in $\text{Ho}_2\text{Ti}_2\text{O}_7$.

the signals have been normalized to the full amplitude found from a so called “indirect alpha” calibration. The non-relaxing component is attributed to the development of a static component of the order of 1 T. It should be pointed out that the muon has no sensitivity to a static internal field once it has been swamped by the high longitudinally applied field and the depolarization function is said to be “decoupled”. Thus in this regime the residual relaxing component observed in 20 kOe is thought to be dynamic by nature. If the muon spin depolarization were due to a static internal field Δ of the order of 1 T, it would take place on a time scale of $\Delta^{-1} \approx 1$ ns, too fast to be observed.

The most dramatic feature of the data taken in a longitudinal field of 20 kOe is the persistent, temperature independent spin relaxation observed below 1 K. Typically, in a conventional system some type of ordered phase would be favoured energetically at low temperature. In a 3 dimensional antiferromagnet below the transition temperature $T_1^{-1} \propto T^3$ for $T \gg T_{AE}$ and $T_1^{-1} \propto T^2 \exp(-T_{AE}/T)$ for $T \ll T_{AE}$, where T_{AE} is the gap in the spin wave spectrum due to anisotropy. In other words, below T_N , T_1^{-1} decreases rapidly as the magnetic excitations freeze out. Though difficult to understand theoretically, such partial ordering with persistent low temperature spin dynamics is a recurring phenomenon in the field of geometrically frustrated magnets.

Experiment 865

Electronic structure and diffusion kinetics of Mu in group III nitrides and related wide-gap semiconductors

(K. Shimomura, R. Kadono, KEK-IMSS)

Since the discovery of methods to produce sufficient *p*-type conductivity by Mg-doping, gallium nitride and related compound semiconductors are be-

ing aggressively developed for electronic and optoelectronic devices such as blue/green lasers and light-emitting diodes. Unique features such as a wide and direct band gap and high breakdown field make the nitrides ideal for such applications. However, as-grown undoped GaN epitaxial thin films, as well as bulk single crystals, commonly exhibit n -type conductivity with concentrations ranging from 10^{16} to 10^{19} cm^{-3} . Extensive experimental and theoretical studies have been undertaken to understand the origin of this n -type conductivity.

Here we report on the first observation of a paramagnetic muonium spectrum in GaN. The observed Mu^0 state has an extremely small and highly anisotropic hyperfine parameter. The location within the band gap for the $[0/+]$ energy level associated with this Mu state is estimated from the measured activation energy for thermal ionization. These results imply that an isolated hydrogen impurity would behave as a shallow donor if it were located at the same crystallographic site.

We performed μSR measurements on a GaN single crystal with the hexagonal (2H) wurtzite structure. The μSR experiment was conducted at the TRIUMF M15 beam line with the Belle spectrometer. Muons from a surface beam with their polarization transverse to the applied magnetic field were implanted into GaN ($[0001]$ orientation, n -type with a concentration of 10^{16} cm^{-3}).

Above 25 K, only a single (diamagnetic) precession signal is observed at the muon Larmor frequency. Relaxation of this signal is well described by Gaussian damping. This damping rate is satisfactorily explained by the dipole-dipole interaction of muons with $^{69,71}\text{Ga}$ and ^{14}N nuclei. The muon spin rotation signal changes drastically below 25 K. Figure 121 shows the angular and temperature dependence of the frequency spectra obtained by Fourier transform, in which one pair of satellite lines is clearly seen with their positions situated symmetrically around the central line, which corresponds to the precession of diamagnetic muons. The splitting of these satellites remained unchanged when the applied field was increased from 1.5 T up to 5 T, a result that is important in identifying the spectra as due to the hyperfine interaction of a Mu^0 centre. The splitting decreases when the $[0001]$ axis is tilted with respect to $\sim B$ as in Fig. 121d. Moreover, an equivalent frequency spectrum was observed when the $[1120]$ axis was rotated around $[0001]$, which was oriented at 35° to the applied magnetic field. These observations demonstrate the presence of a paramagnetic muonium state in GaN. The resulting hyperfine interaction is extremely small, about 10^{-4} times the vacuum value for a Mu atom, and is axially symmetric with respect to $[0001]$.

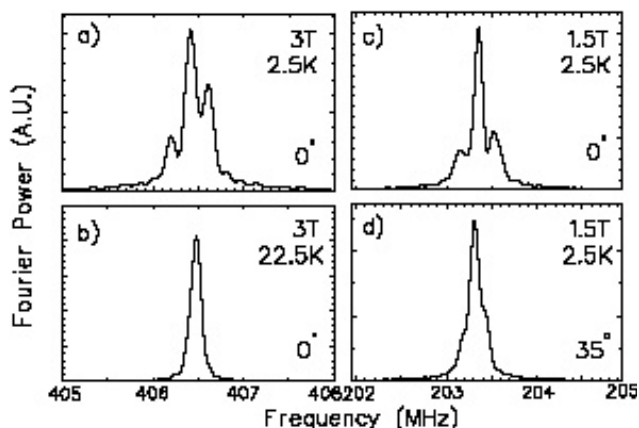


Fig. 121. Frequency spectra obtained for GaN at (a) 2.5 K and (b) 22.5 K with $B = 3.0$ T parallel to $[0001]$ axis, and with $B = 1.5$ T at 2.5 K, where $[0001]$ is parallel to B (c) or tilted by 35° from B (d).

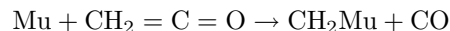
Because the population of the $Se = -1/2$ state is always larger in an applied field, the observations in Fig. 121 imply that the low-frequency line corresponds to $Se = +1/2$, thus to $A(\mu)$ is positive for the displayed orientations. From the detailed analysis, the parallel and perpendicular component of the hyperfine tensor is deduced to be $+337(10)$ kHz and $-243(30)$ kHz, respectively.

The temperature dependence measurement of the Mu^0 state shows their activation energy to be about 5 meV.

Experiment 883

Muoniated methyl and associated free radicals (P.W. Percival, SFU)

After an exciting excursion into a study of radicals formed from addition of muonium to stable carbenes [McKenzie *et al.*, J. Am. Chem. Soc. **125**, 11565 (2003)], Expt. 883 returned to its original focus in 2003, being a detailed study of the muoniated methyl radical, $\cdot\text{CH}_2\text{Mu}$, and its isotopomers. The first step in this project was to find a method of creating the radical. This was achieved by using ketene as the radical precursor:



as reported in the 2001 TRIUMF Annual Report and a subsequent paper [McKenzie *et al.*, J. Phys. Chem. **A106**, 7083 (2002)].

The new work involved the deuterated analogue, $\cdot\text{CD}_2\text{Mu}$, formed by addition of muonium to $\text{CD}_2=\text{C}=\text{O}$. Neither ketene nor deuteroketene are available commercially, since they are highly unstable molecules. Thus it was necessary to prepare fresh samples (by the pyrolysis of acetone or deuterioacetone) just prior to beam time, and store them in dry ice prior to

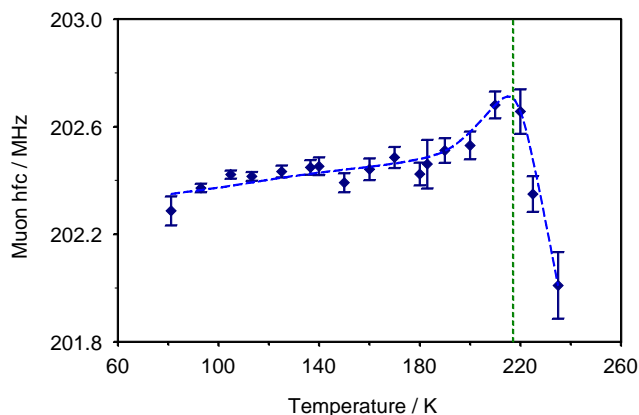


Fig. 122. Muon hyperfine constants determined for the $\cdot\text{CD}_2\text{Mu}$ radical. The dotted vertical line marks the boiling point of the ketene solvent.

mounting in a pre-cooled cryostat. As before, muon hyperfine constants were determined by transverse field μSR and proton or deuteron hyperfine constants were determined by muon level-crossing resonance, μLCR . Measurements were made over a wide range of temperature, from about 70 K to over 230 K, where the ketene dimerizes and it is no longer possible to form the muoniated methyl radical of interest.

The intent was to study the temperature dependence of the hyperfine constants and their isotopic dependence, to probe details of the vibrational motion of the radicals, specifically the out-of-plane (umbrella) bending motion, which is supposed to be the main cause of temperature dependence for the proton hyperfine coupling in the $\cdot\text{CH}_3$ radical. However, the effect of temperature was unexpectedly small for $\cdot\text{CH}_2\text{Mu}$ and $\cdot\text{CD}_2\text{Mu}$, a finding which can now be explained by the high frequency of the inversion mode for the muoniated radicals, as revealed by detailed quantum calculations.

The small temperature dependence of the hyperfine constants is probably due to solvent effects. In particular the significant feature observed near 220 K can be attributed to reduced intermolecular interactions close to the boiling point of ketene (217 K) and the subsequent formation of the dimer, which is itself solid at these temperatures (see Fig. 122).

The muon spin relaxation rate was also measured in the transverse field μSR experiments; the results for $\cdot\text{CD}_2\text{Mu}$ are shown in Fig. 123. The effective activation energy is too small for the relaxation to be due to chemical reaction. On the other hand the sign of the temperature dependence is opposite to that found for most organic free radicals, and which is usually attributed to the modulation of anisotropic g and hyperfine interactions by molecular tumbling. It is therefore concluded that the spin relaxation must be due to the spin-rotation mechanism, which only becomes dominant for small radicals undergoing very rapid

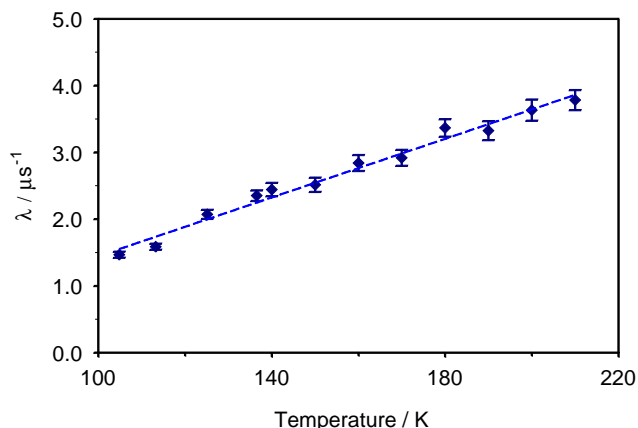


Fig. 123. Transverse muon spin relaxation rates measured for the $\cdot\text{CD}_2\text{Mu}$ radical in liquid ketene.

tumbling and would apply to the small, oblate shape of the methyl radical.

The research carried out in Expt. 883 forms a major part of the Ph.D. thesis of Iain McKenzie (Chemistry Department, Simon Fraser University, in press).

Experiment 895

Vortex structure and magnetism of electron-doped cuprate superconductors

(*R. Kadono, K.M. Kojima, KEK-IMSS, Tokyo*)

Recent observation of field-induced magnetism (FIM) in the mixed state of hole-doped (p -type) cuprates has attracted much interest, because it might provide a clue to resolve the true ground state in the normal phase of those compounds. Since the superconducting order parameter is locally suppressed in the vortex cores, there is a possibility that FIM may be a manifestation of the electronic ground state nucleated in the normal cores. However, while all of the observed effects are attributed to the antiferromagnetic (or quasistatic stripe) phase localized in the vortex cores, the evidence for the “antiferromagnetic (AF) core” remains elusive; for example, the results in $\text{La}_{2-x}\text{Sr}_x\text{CuO}_4$ [Katano *et al.*, Phys. Rev. **B62**, R14677 (2000); Lake *et al.*, Science **291**, 1759 (2001); Nature **415**, 299 (2002)] are all from neutron diffraction measurements which are not sensitive to the local structure over such a large length scale (vortices with a core size of $\sim 10^2$ Å, separated by 10^2 – 10^3 Å). The situation is less clear in electron-doped (n -type) cuprates because the information related with vortices is often masked by the influence of large magnetic moments of rare-earth ions in $R_{2-x}\text{Ce}_x\text{CuO}_4$ ($R = \text{Nd, Pr, Sm}$).

In 2003 we performed detailed high transverse field (TF) μSR measurements on the single crystalline n -type cuprate $\text{Pr}_{1-x}\text{LaCe}_x\text{CuO}_{4-y}$ (PLCCO) to study the mixed state. A specimen with $x = 0.11$, which is relatively close to the AF phase of PLCCO ($x \leq 0.1$), was chosen to examine the possibility of FIM. For

the study of FIM, PLCCO has an advantage over $\text{Pr}_{2-x}\text{Ce}_x\text{CuO}_{4-y}$ (PCCO) in that we can obtain single crystals in much larger dimensions, which allows systematic studies by various experimental techniques including neutron diffraction. The μSR measurements were carried out on the M15 beam line. A slab of $\text{Pr}_{0.89}\text{LaCe}_{0.11}\text{CuO}_{4-y}$ crystal ($T_c \simeq 26$ K, measuring about $5 \times 8 \times 0.5$ mm) with the c axis perpendicular to the plane was loaded onto a He gas-flow cryostat and a magnetic field ($\mathbf{H} = (0, 0, H_z)$) was applied parallel to the c axis (where $z \parallel c$). In the paramagnetic state, we have found that the muon Knight shift, K_μ^z , under an external magnetic field parallel to the c axis is significantly influenced by the in-plane susceptibility, χ_{ab} . This surprising result strongly suggests the presence of unconventional hyperfine interaction involving a non-diagonal Fermi contact-type term between muons and Pr ions. The muon hyperfine parameter A_μ^z is deduced from a comparison between the muon Knight shift and magnetic susceptibility χ . As shown in Fig. 124a, PLCCO exhibits a large anisotropy of χ between the in-plane (χ_{ab}) and perpendicular (χ_c) directions, where χ_{ab} exhibits a significant increase with decreasing temperature while χ_c remains almost unchanged. The corresponding muon Knight shift versus temperature is shown in Fig. 124b; it is clear that K_μ^z is mostly proportional to χ_{ab} . The K - χ plot in Fig. 124c for the data obtained in the normal state exhibits a linear relation with a small offset near the origin, from which we obtain $-969(2)$ Oe/ μ_B corresponding to the gradients of the K - χ line. Upon superconducting transition, the specimen exhibits a further peculiar magnetic response. As is evident in Fig. 125, showing the field dependence of the additional shift in the superconducting state, $\Delta B_z = B_0^S - B_0^N$, a large positive shift of the frequency is observed at $H = 200$ Oe. Note that the direction of the frequency shift is apparently opposite to that expected for diamagnetism in the mixed state. This result is quite similar to what has been observed in PCCO [Sonier *et al.*, Phys. Rev. Lett. **91**, 147002 (2003)]. Moreover, ΔB_z exhibits a steep decrease with increasing field to change its sign to negative above ~ 1 kOe. The strong field dependence at such low fields indicates that the effect of diamagnetism due to flux line lattice (FLL) is negligible over the entire field range. Meanwhile, ΔB_z is only weakly dependent on the field for 2–40 kOe, above which it exhibits a trend to increase further in the negative direction. These features above ~ 2 kOe are quite similar to those of field-induced moments detected by neutron diffraction. The field dependence of ΔB_z for $H \leq 40$ kOe can be understood by introducing an additional polarization of Pr and/or Cu moments that is controlled by the superconductivity. Assuming a simple Brillouin function for the

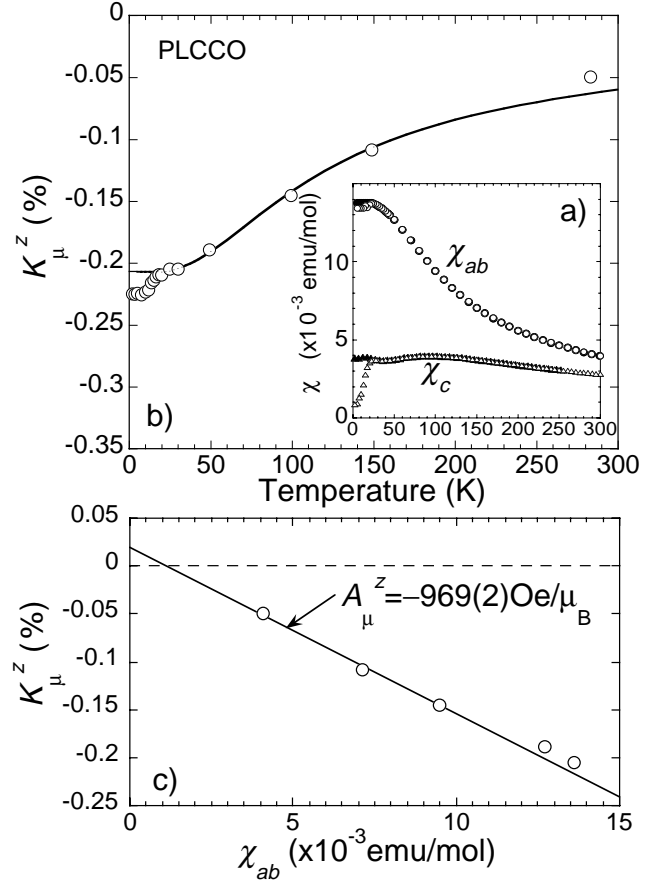


Fig. 124. (a) Temperature dependence of magnetic susceptibility at $H = 20$ kOe (open symbols) and 50 kOe (filled symbols) applied parallel (χ_c) and perpendicular (χ_{ab}) to the c axis. (b) The muon Knight shift with $H = 20$ kOe parallel to the c axis, where the solid curve in (b) is proportional to χ_{ab} . (c) The K - χ plot (with $\chi = \chi_{ab}$) for the Knight shift shown in (b).

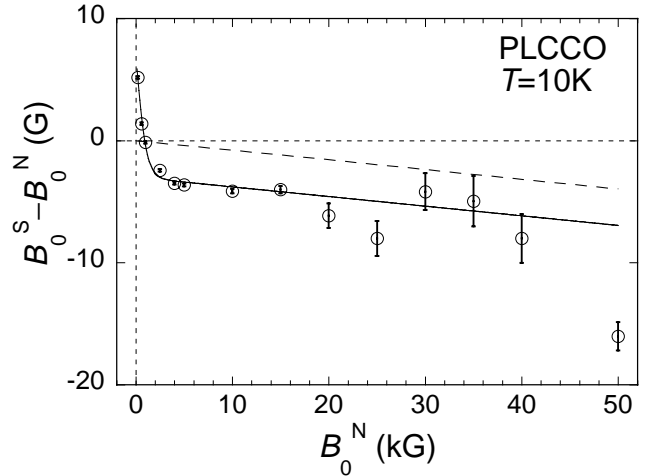


Fig. 125. Magnetic field dependence of the additional shift in the superconducting state, where B_0^S and B_0^N correspond to the internal field at 10 K and 30 – 40 K, respectively. The solid curve is a fitting result by the model described in the text (with the dashed line representing the contribution of residual demagnetization).

magnetic response, we analyze the data in Fig. 125 by an equation

$$\Delta B_z = B_z^* \tanh(H_z/H_p) + c_{\text{dm}} H_z + b_0,$$

where B_z^* is the field from the additional moment, H_p is a characteristic field where the direction of B_z^* is reversed, c_{dm} is the contribution of residual bulk demagnetization, and b_0 is an offset parameter. The solid curve in Fig. 125 is a result of fitting by the above equation, which reproduces data excellently with $B_z^* = 9.78(8)$ Oe, $H_p = 1.09(4)$ kOe, $c_{\text{dm}} = -7.9(1.4) \times 10^{-5}$, and $b_0 = 6.8(2)$ Oe. Since the emergence of B_z^* is perfectly correlated with the occurrence of superconductivity, the origin of B_z^* must be in close relation with the electronic state of CuO_2 planes. However, it has been demonstrated by very recent neutron diffraction measurements on the present specimen that the moment size of Cu ions induced by the external field is far smaller than that found in the AF phase of $\text{Pr}_{1-x}\text{LaCe}_x\text{CuO}_{4-y}$ ($x < 0.1$) with a quite non-linear dependence on the field; it remains almost constant over a range from 0 to ~ 40 kOe. Considering the hyperfine coupling between Cu ions and muons at the relevant site (which is usually dominated by magnetic dipolar interaction), it is unlikely that such small Cu moments directly contribute to B_z^* , in contrast to what has been suggested for the case of PCCO. Further analysis is still in progress.

Experiment 914/835

Zero-field μSR in Bi2212 and Bi2201 searching for effects related to pseudo-gap

(G.M. Luke, McMaster; P.L. Russo, Y.J. Uemura, Columbia)

In Expt. 914/835, we performed TF-MuSR measurements of Bi2201 in the underdoped, optimally doped, and overdoped regimes using mildly oriented ceramic specimens. Our initial motivation came from the work of Balakirev *et al.* [Nature **424**, 912 (2003)], who have performed Hall number measurements by suppressing superconductivity using high magnetic fields, and reported that the carrier concentration $n_{\text{Hall}} \sim 1$ hole per Cu at the optimum doping, as shown in Fig. 126. In most of the cuprates, it has been widely believed that the carrier concentration at optimum doping region is close to 0.15 holes per Cu. So, $n_{\text{Hall}} \sim 1$ in Bi2201 is anomalously large by a factor of 6 or so.

When we plot the μSR relaxation rate, which is proportional to n_s/m^* (superconducting carrier density / effective mass), versus T_c , Bi2201 systems follow the trend of various other cuprate systems, as shown in Fig. 127. Bi2201 has an average spacing $c_{\text{int}} \sim 12$ Å of CuO_2 planes, which is twice as large as $c_{\text{int}} \sim 6$ Å of 214, 123, and most other cuprate systems. Thus when

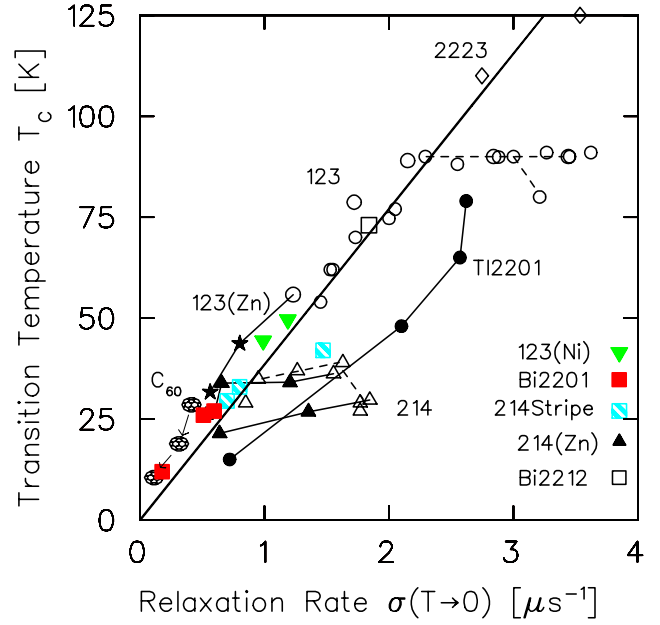


Fig. 126. Uemura plot updated with Bi2201 and Bi2212.

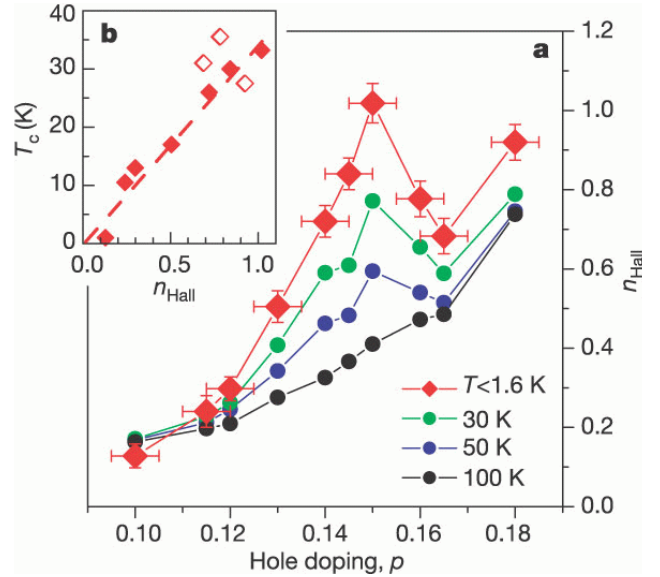


Fig. 127. Variation of Hall number with doping and T_c . **a**, Hall number (n_{Hall}) variation with doping (p). **b**, low temperature (n_{Hall}) and T_c for underdoped samples with $p \leq 0.15$ [Balakirev *et al.*, *op. cit.*].

we convert the results in Fig. 127 into a 2-dimensional superfluid spectral weight $n_{s2d}/m^* \propto \sigma \times c_{\text{int}}$, we expect about a factor 2 larger carrier density per Cu for Bi2201 compared to other cuprates, assuming that m^* values are nearly equal for all these systems. This is still not enough to account the factor ~ 6 anomaly.

Therefore, our results are not consistent with the anomaly of Hall number measurements unless, (1) the effective mass in Bi2201 is anomalously large, or (2) the

derived n_{Hall} somehow does not represent real carrier concentration.

Future plans

We are now checking the alignment of crystallites and developing a method to convert the relaxation rate to corresponding values for single crystal specimens. We would like to perform measurements using single crystal specimens of Bi2212 in several different applied fields in the future.

Experiment 915

Muonium in semiconductor alloys

(P.J.C. King, Rutherford Appleton Laboratory)

Experiment 915 has focused on investigation of muonium behaviour in $\text{Si}_{1-x}\text{Ge}_x$ alloys. Strained-layer $\text{Si}_{1-x}\text{Ge}_x$ alloys, grown epitaxially on to Si or SiGe substrates, have applications in transistor manufacture and provide the prospect of combining Si integrated circuit technology with optoelectronic components. The uses of epitaxial $\text{Si}_{1-x}\text{Ge}_x$ material have generated interest in the bulk, unstrained alloy, and this can be produced by the Czochralski technique in wafer form. Bulk alloy material offers the opportunity to study the intrinsic physical and electronic properties of the $\text{Si}_{1-x}\text{Ge}_x$ system. For example, regarding impurity behaviour within the system, the lattice site of dissolved oxygen has been investigated [Yonenaga *et al.*, Physica **B308-310**, 539 (2001)], with this species showing a preference for adopting a bond-centred location within Si-Si bonds. There have also been limited studies of hydrogen behaviour: DLTS investigations of very dilute (<1% Ge) material showed some modification of the properties of bond-centred hydrogen due to local variations in its environment; at the other end of the alloy spectrum, there is some evidence for the electrical activation of impurity Si atoms in Ge by hydrogen. The aim of this present experiment was to explore the behaviour of isolated hydrogen in bulk $\text{Si}_{1-x}\text{Ge}_x$ across the alloy composition, as modelled by its muonium analogue.

In November, 2001, three alloy compositions (Ge content 20%, 45%, 77%) were studied on M15 using the Belle magnet; these Czochralski samples were grown at Tohoku University. Qualitatively, the Mu_{BC} and Mu_{T} formation probabilities vary smoothly across the alloy range between the fractions expected in the unalloyed elements. Mu_{BC} was observed in all three samples and a linear variation of the average value of the isotropic component of its hyperfine parameter as a function of alloy composition was observed. The Mu_{BC} lines were broad, however, and further investigation of their nature was required. Mu_{T} signals were only seen in the alloy with 20% Ge content. The measured Mu_{T} hyperfine parameter was lower than that observed in pure Si

(whereas linear interpolation between the pure Si and Ge values suggests a higher value), and further investigation of the Mu_{T} hyperfine parameter in other low-Ge samples was of interest to confirm this behaviour.

In October, 2003 three $\text{Si}_{1-x}\text{Ge}_x$ samples were studied during low-intensity running at the start of a TRIUMF run cycle: Czochralski material with 11% Ge content from Virginia Semiconductor, material with 60% Ge content from Tohoku, and material with 20% Ge content which had been investigated previously.

In the 11% Ge material, both Mu_{BC} and Mu_{T} signals could be clearly seen. Figure 128 shows the asymmetries as a function of temperature for the two paramagnetic species together with the diamagnetic amplitude. This latter component is small and constant below around 150 K, above which it begins to increase due to Mu_{BC} ionization; the Mu_{T} amplitude remains constant above 20 K up to at least 230 K. However, both paramagnetic centres show a large dip in amplitude around 10 K, and the origin of this behaviour requires further exploration.

Material with 60% Ge content was studied very briefly in a single run; a Mu_{BC} line could be seen, and there is also some evidence for a Mu_{T} signal. Figure 129 shows a plot of the average value of Mu_{BC} hyperfine parameter versus alloy composition with the results from the 11% and 60% Ge samples added. Whilst the data point for 60% Ge has not benefited from the higher statistics that the other points had, the linear dependence on alloy composition is confirmed.

Figure 130 shows the Mu_{T} hyperfine parameter versus temperature as measured previously for the 20% Ge sample, together with new TRIUMF measurements for the 11% Ge sample. The parameter values are very similar between these two samples and below that expected for pure Si. For the 20% Ge case, there is the hint of a minimum in hyperfine parameter around 40 K; this is shown more clearly in the 11% Ge case.

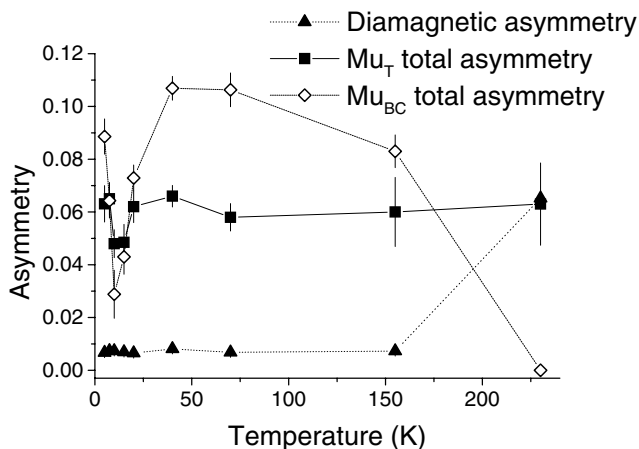


Fig. 128. Mu_{BC} , Mu_{T} and diamagnetic line asymmetries as a function of temperature from $\text{Si}_{0.89}\text{Ge}_{0.11}$.

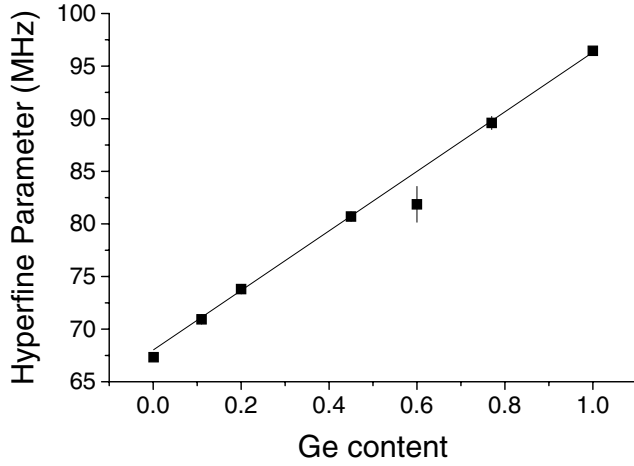


Fig. 129. Variation of the average value of the isotropic component of the Mu_{BC} hyperfine parameter with alloy composition. The line is a fit to the data.

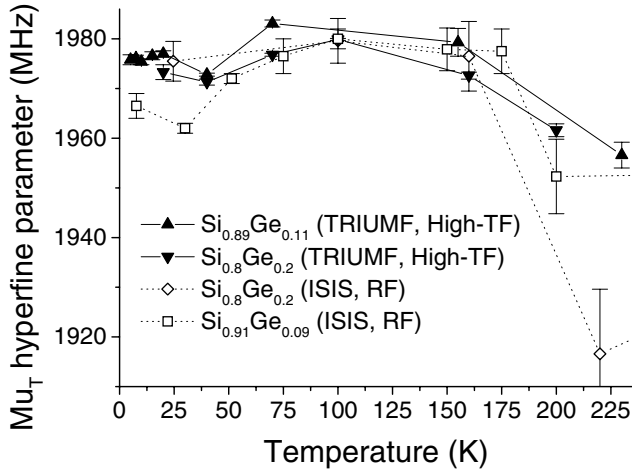


Fig. 130. Mu_{T} hyperfine parameter for different alloys measured either using high transverse fields at TRIUMF or RF- μ SR at ISIS.

Also shown in this figure are data from ISIS, where the Mu_{T} hyperfine parameter has been measured using radio-frequency resonance methods. Data from the 20% Ge sample agree closely with that taken at TRIUMF and measured using the high transverse field technique. In addition, ISIS data from a sample from Tohoku with 9% Ge are shown – these show a more pronounced fall in hyperfine parameter below 100 K, again with a minimum suggested at around 30 K.

The observed temperature dependence of the Mu_{T} parameter at low temperatures in these alloys is of interest. In pure Si, the Mu_{T} hyperfine constant decreases with falling temperature below around 75 K. Holzschuh [Phys. Rev. **B27**, 102 (1983)] attributed this decrease to Mu_{T} hopping between sites with slightly different isotropic hyperfine interactions. At low temperatures, these sites are populated according to the Boltzmann distribution which would preferentially give

more weight to those with lower hyperfine parameters. In low Ge alloy material, it might be expected that this effect would be greater, there being a wider possible variation in Mu_{T} sites owing to different numbers of Ge atoms surrounding cage centres. This may account not only for the fall in Mu_{T} hyperfine parameter with decreasing temperature below around 100 K, but also the low overall value compared with Si.

Further study of the data is ongoing. In particular, quantitative analysis of the variation with temperature of the Mu_{T} hyperfine parameter needs to be performed; in addition, high statistics data were also taken for the 20% Ge sample, and analysis to look for preferential occupation of specific bonding environments is proceeding.

Experiment 916

QLCR of diamagnetic muonium states in GaP (R.L. Lichti, Texas Tech)

Zero-field depolarization functions demonstrated that several different diamagnetic muonium states exist in doped GaP. The primary goal of TRIUMF Expt. 916 has been identification of these states using quadrupolar level-crossing resonances (QLCR). The two Ga isotopes produce a clear signature of a Ga near neighbour to the muon by nearly identical features at a field ratio of ~ 1.6 , while P has no quadrupolar nuclei, and thus is invisible to this technique. The standard Zn acceptor in GaP substitutes for Ga and has only a 4.1% fraction with a nuclear quadrupole moment, while the usual S donor has no quadrupolar isotope. The S donor will not be visible, but a small possibility exists that a Zn acceptor might be observed in QLCR experiments.

We have previously found the main Ga-related resonances associated with the Mu^+ defect centre at the bond-centre (BC) site in *p*-type GaP, and confirmed that the intensity of that spectrum decreases below roughly 100 K where the zero-field depolarization results indicate formation of a bound Mu-Zn pair. The Mu_{BC}^+ QLCR resonances lie between 200 and 400 mT and imply an electric field gradient (EFG) at the Ga that is roughly 10% larger for Mu^+ in GaP compared to that for the same state in GaAs. One of the remaining measurements for Expt. 916 beam time in late summer was to verify that a different resonance occurs below 100 K due to the Mu-Zn complex. We have observed a weak low-field Ga resonance at 670 K where a Mu-Zn complex is formed by Coulomb capture of the mobile Mu^+ by an ionized Zn^- acceptor. A major question is whether the structure of the Mu-Zn pair is identical at high and low temperatures, where the proposed process involves charge-exchange scattering between the mobile Mu_{T}^0 centre and a neutral Zn

acceptor as the first step toward pair formation.

Figure 131a shows the low-field QLCR spectrum obtained in heavily doped *p*-type GaP at 50 K. These resonances are too strong to be from Zn and very similar to the Ga spectrum seen at 670 K except that it is shifted to higher fields, implying that the EFG at nearby Ga nuclei is about 20% larger at 50 K than for the high-temperature complex. This result would seem to indicate that the Mu-Zn pair structure is very similar at these two temperatures. The fact that the same resonances are not seen in Fig. 131b at a temperature where Mu_{BC}^+ remains stationary, but the low-temperature pair formation process is not active because the Zn acceptors have ionized, shows that this spectrum is from a separate low-T state rather than due to the second-nearest Ga neighbours to Mu_{BC}^+ . Since the usual structure for an H-acceptor complex has the hydrogen in a BC location next to the acceptor, these results suggest that the structure of Mu-Zn is most likely not the standard one. We proposed a pair

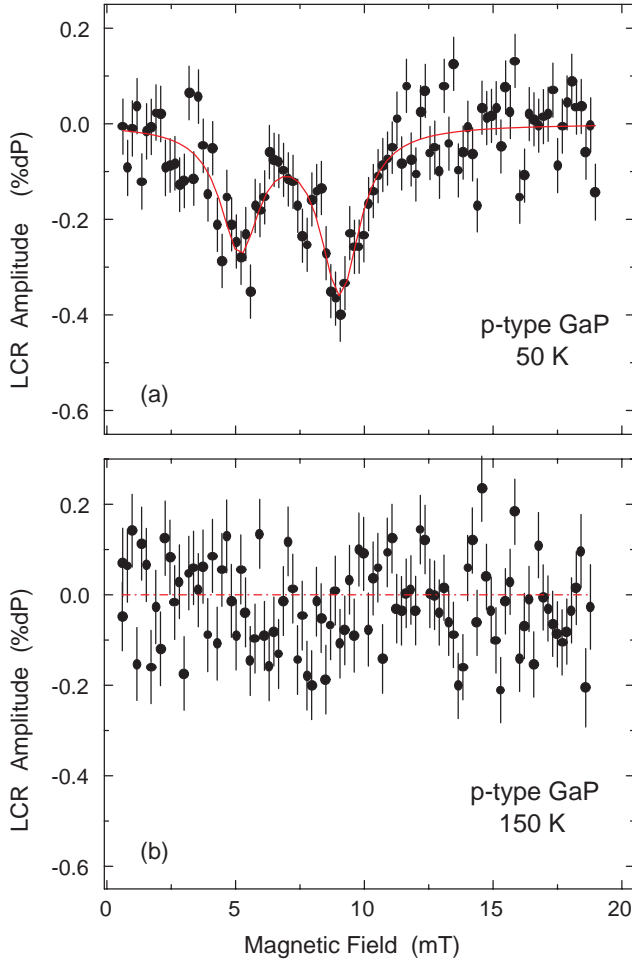


Fig. 131. QLCR spectra for Ga neighbours to the Mu location in a Mu-Zn complex formed at low temperatures (a). A similar scan (b) above the maximum temperature for low-T pair formation confirms a separate low-T state.

structure at high temperatures in both GaP and GaAs in which the Mu^+ resides behind the As or P neighbour to Zn_{Ga} , or is mobile among P-Ga (As-Ga) bonds one step removed from the Zn dopant as an explanation for these low-field resonances.

Figure 132 shows the spectrum obtained at 300 K in a heavily doped *n*-type GaP sample. We had previously identified Mu^- at 140 K where there is a peak in the diamagnetic fraction; however, the temperature dependence of that fraction was not as expected. Thus confirming Mu^- at the Ga tetrahedral location near room temperature became one of our goals for the most recent beam time as an identity check for a diamagnetic state that grows roughly linearly between 200 and 700 K. The resonance in Fig. 132 is essentially identical to that seen at 140 K, except for a small shift in the resonance fields. The odd dependences seen in *n*-type GaP above 100 K thus appear not to involve any state other than Mu^- .

We have now confirmed our preliminary identification of four of the five proposed diamagnetic states in doped GaP; Mu^- at T_{Ga} , Mu^+ at BC, a high-temperature Mu-Zn paired state formed by Coulomb capture of mobile Mu^+ by Zn^- , as well as the low-temperature Mu-Zn paired state formed by charge-transfer interactions between mobile Mu_T^0 centres and neutral Zn acceptors which is discussed above. The one remaining state is a low-temperature Mu-donor complex which should have the Mu located in a tetrahedral location surrounded by P atoms next to the S donor. An initial attempt did not find any low-field spectrum; however, this was not an exhaustive search. The expected structure is the least likely of all the proposed diamagnetic Mu centres to yield a QLCR signature in

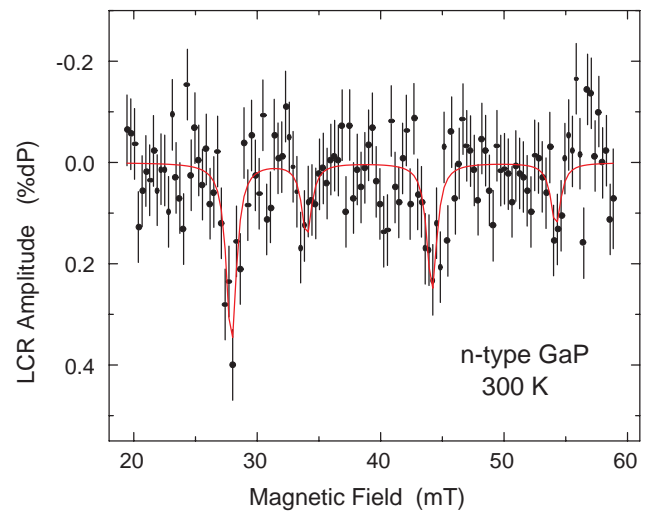


Fig. 132. QLCR spectra confirm Mu^- in the T_{Ga} site at 300 K for heavily doped *n*-type GaP. The electric field gradient at a Ga neighbour is slightly smaller at 300 K than at 140 K where the Mu^- fraction is larger.

GaP. Based on identification of a standard Mu^- centre as the main state at both 140 and 300 K, we conclude that the unusual dependences observed for diamagnetic fractions above 100 K may be the result of competing transitions out of the Mu_T^0 precursor to Mu^- . Answering that question requires a careful study of Mu_T^0 dynamics in n -type GaP which is being pursued as part of a separate experiment to define Mu defect energy levels in III-V compounds.

Experiment 917

Correlation between magnetism and transport properties of thermoelectric oxides

(J. Sugiyama, Toyota CRDL Inc.; J.H. Brewer, UBC-TRIUMF)

Although the widespread current interest in the layered cobaltites (i.e. 5 K superconductivity in $\text{Na}_{0.35}\text{CoO}_2 \cdot \text{H}_2\text{O}$ [Takada *et al.*, Nature **422**, 53 (2003)] was originally due mainly to their unique combination of high thermopower S with metallic transport properties, which makes them one of the most promising systems for power applications, we have shown that they also display interesting and complex magnetic orderings, directly correlated with the enhanced S . The richness of behaviour of the layered cobaltites is due to their intrinsic structure, namely: electrically active triangular planes of CoO_2 , which are separated by a variety of intermediate structures; their relatively strong electronic correlations; and the fact that the structures between the CoO_2 planes can be modified in a variety of ways to vary their dimensionality, ionic states, carrier doping in the CoO_2 planes and the relevant interaction strengths.

In order to elucidate the magnetism in the CoO_2 planes and the mechanism of the good thermoelectric properties, we have carried out positive muon spin rotation and relaxation ($\mu^+\text{SR}$) experiments on the layered cobaltites. As a result, we found the transition to a low- T commensurate or incommensurate spin density wave (C- or IC-SDW) state for $[\text{Ca}_2\text{CoO}_3]_{0.62}^{\text{RS}}[\text{CoO}_2]$ below ~ 100 K, [Sugiyama *et al.*, Phys. Rev. **B66**, 134413 (2002); *ibid.* **68**, 134423 (2003)], $\text{Na}_{0.75}\text{CoO}_2$ at 22 K [Sugiyama *et al.*, *ibid.* **67**, 214420 (2003)] and $[\text{Ca}_2\text{Co}_{4/3}\text{Cu}_{2/3}\text{O}_4]_{0.62}^{\text{RS}}[\text{CoO}_2]$ below ~ 200 K [Sugiyama *et al.*, J. Phys. Condens. Matter **15**, 8619 (2003)], where RS denotes the rocksalt-type subsystem. Here we summarize those results and report an almost dome-shaped relation between the transition temperature into the low- T magnetic state and the composition x for Na_xCoO_2 and/or the high-temperature asymptotic limit of thermopower in the more complex 3 and 4 layer cobaltites [Sugiyama *et al.*, Phys. Rev. Lett. **92**, 017602 (2004)]. This behaviour is explained using the Hubbard model on two-

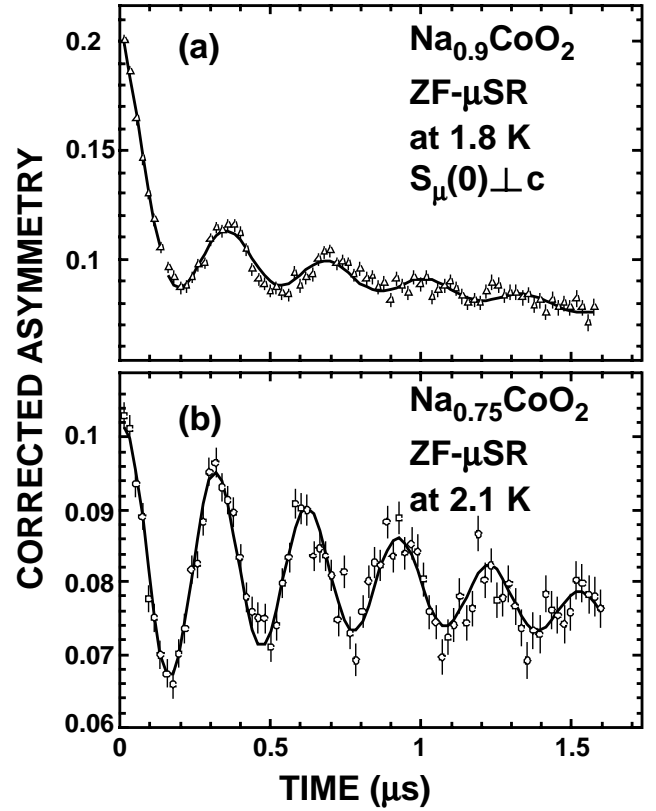


Fig. 133. ZF- $\mu^+\text{SR}$ time spectra of (a) single crystal platelets of $\text{Na}_{0.9}\text{CoO}_2$ at 1.8 K and (b) a polycrystalline plate of $\text{Na}_{0.75}\text{CoO}_2$ at 2.1 K.

dimensional triangular lattice in the CoO_2 plane.

Figure 133(a) shows a ZF- $\mu^+\text{SR}$ time spectrum at 1.8 K in the single crystal platelets of $\text{Na}_{0.9}\text{CoO}_2$; the spectrum was obtained with the initial μ^+ spin direction $\mathbf{S}_\mu(0)$ perpendicular to the c -axis. A clear oscillation due to quasi-static internal fields is observed only when $\mathbf{S}_\mu(0) \perp \mathbf{c}$. Also, the ZF- $\mu^+\text{SR}$ time spectrum for the polycrystalline $\text{Na}_{0.75}\text{CoO}_2$ sample, which entered a commensurate spin structure below 22 K, is shown in Fig. 133(b). Making comparison with the bottom spectrum, the oscillation amplitude in the top spectrum decays rapidly and the initial phase is delayed. The oscillation in the top spectrum is characteristic of a zeroth-order Bessel function of the first kind that describes the muon polarization evolution in an IC-SDW field distribution [Kalvius *et al.*, Handbook on the Physics and Chemistry of Rare Earths (North-Holland, Amsterdam, 2001) vol. 32, chap. 206]. The absence of a clear oscillation for the $\mathbf{S}_\mu(0) \parallel \mathbf{c}$ case indicates that the internal field is roughly parallel to the c -axis. Due to the strong anisotropy, the IC-SDW is thus considered to localize in the CoO_2 plane, with oscillating moments directed along the c -axis.

The magnetic phase diagram (Fig. 134) of Na_xCoO_2 can thus be sketched from the $\mu^+\text{SR}$ results

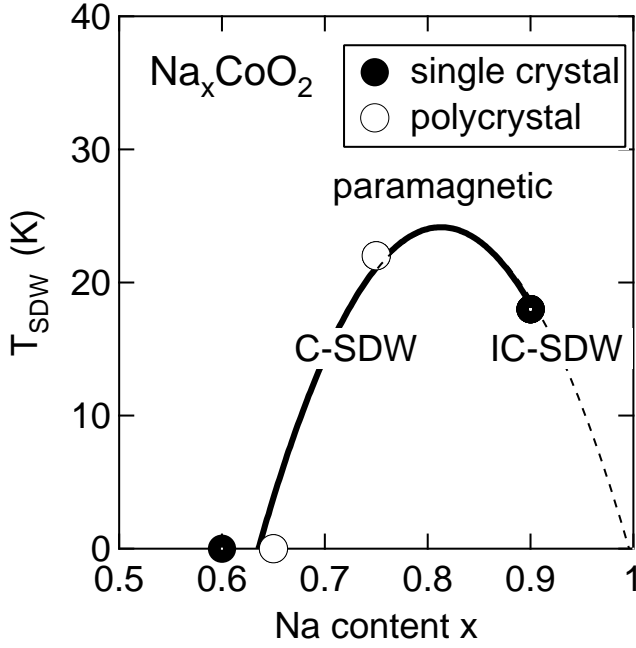


Fig. 134. Phase diagram of Na_xCoO_2 determined by the $\mu^+\text{SR}$ experiments. The point at $x = 1$ is extrapolated from the data on the related compound LiCoO_2 .

for polycrystalline samples with $x = 0.65$ and 0.75 and the $x = 0.6$ and 0.9 crystals. Since the oxygen deficiency δ in $\text{Na}_x\text{CoO}_{2-\delta}$ is negligibly small even for the $x = 0.9$ sample, the average Co valence is directly calculated from x . As x increases from 0.6 , the magnitude of T_{SDW} increases up to $x \sim 0.8$, then decreases with further increasing x . As a result, we obtain the dome-shaped relationship of Fig. 134 between T_{SDW} and x , viz. the Co valence for Na_xCoO_2 .

The Hubbard model within a mean field approximation can be used for explaining the magnetism of such a system as a function of electron filling n . At $T = 0$ and $n = 0.5$ (i.e. Na_0CoO_2), as the Hubbard on-site repulsion U increases from 0 , the system is a paramagnetic (PM) metal up to $U/t = 3.97$ due to geometrical frustration, then changes into a metal with a spiral IC-SDW, and then at $U/t = 5.27$ a first-order metal-insulator transition occurs, where t is the nearest-neighbour hopping amplitude [Krishnamurthy *et al.*, Phys. Rev. Lett. **64**, 950 (1990)]. The lack of magnetic transitions for Na_xCoO_2 with $x = 0.6$ and 0.65 suggests that $U/t \leq 3.97$. This means that Na_xCoO_2 is unlikely to be a typical strongly correlated electron system, because $U \gg t$ for such a system.

The calculations [Fujita *et al.*, J. Phys. Soc. Jpn. **60**, 2831 (1991)] also predict that, as n increases from 0 , the value of U/t at the boundary between the PM and SDW phases decreases, with increasing slope ($d(U/t)/dn$) up to $n = 0.75$. Even for $U/t = 0$, the SDW phase is stable at $n = 0.75$. The value of U/t then increases with further increasing n , with decreas-

ing slope. Therefore, the dome-shaped phase diagram is qualitatively explained by the calculations, although the measured maximum of the dome is located around $x = 0.8$ (i.e. $n = 0.9$). This is likely due to the simple band structure assumed in the above calculation, while calculations for Na_xCoO_2 suggest a more complicated one [Singh, Phys. Rev. **B61**, 13397 (2000)].

For the 3 and 4 layer cobaltites, $[\text{Ca}_2\text{CoO}_3]_{0.62}^{\text{RS}}[\text{CoO}_2]$ and $[\text{Ca}_2\text{Co}_{4/3}\text{Cu}_{2/3}\text{O}_4]_{0.62}^{\text{RS}}[\text{CoO}_2]$, the IC-SDW transition was also observed as a common behaviour in the CoO_2 planes. We have studied by $\mu^+\text{SR}$ the dependence of the IC-SDW transition on the Co valence for the variety of layered cobaltites. Figure 135 shows $T_{\text{SDW}}^{\text{on}}$ as a function of $S(300 \text{ K})$ for all the cobaltites measured. A clear dome-shaped relation is observed for all the available cobaltites with a variable number of layers (N) between the two adjacent CoO_2 planes. As N increases from 1 , the $T_{\text{SDW}}^{\text{on}} - S(300 \text{ K})$ curve shifts towards higher T , due to the increased two-dimensionality induced by the increase in the interlayer distance between CoO_2 planes.

Phenomenologically, the phase diagram is very similar to the well-known relationship between the superconducting T_c and the Cu valence in the high- T_c cuprates. Actually, both SDW and superconducting transitions are induced by an intrinsic instability of an electron system; that is, as T decreases, an energy gap appears at T_{SDW} and/or T_c to minimize the internal energy for both cases. Therefore, it is reasonable to expect a similar relationship between transition temperature and carrier concentration for both the magnetic cobaltites and the superconducting cuprates.

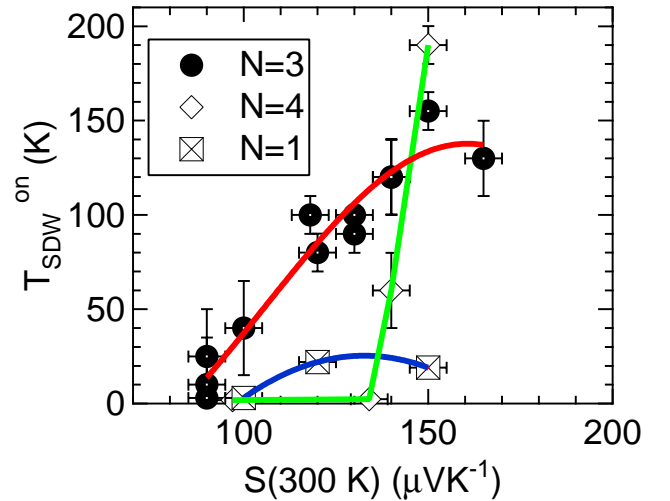


Fig. 135. The relationship between $T_{\text{SDW}}^{\text{on}}$ and thermopower S at 300 K . Solid circles represent the data for the cobaltites with a triple rocksalt-type subsystem, open diamonds a quadruple rocksalt-type subsystem and crossed squares Na_xCoO_2 . It should be noted that the magnetic susceptibility $\chi(T)$ curves for the 3- and 4-layer samples lacked a marked change at the $T_{\text{SDW}}^{\text{on}}$ detected by $\mu^+\text{SR}$.

Furthermore, the average Co valence for the maximum T_{SDW} indicates the optimal filling to induce an SDW transition at high T and enhance the effective mass of charge carriers through the AF interaction between spins. In other words, this dome relation provides important guidance in the search for improved thermoelectric properties of the layered cobaltites.

Experiment 918

High field study of La_2CuO_4 based superconductors

and Experiment 950

High field study of Zn doped/Eu doped/overdoped systems

(G.M. Luke, McMaster; Y.J. Uemura, A.T. Savici, Columbia)

In the previous report for Expt. 918 we showed an increased relaxation rate for the high transverse magnetic field μSR signal in the case of underdoped and optimally doped $\text{La}_{2-x}\text{Sr}_x\text{CuO}_4$ (LSCO). We observed no such effect in the overdoped sample or in the $\text{Bi}_2\text{Sr}_2\text{CaCu}_2\text{O}_{7-\delta}$ (Bi2212) one. We used a new way to look at the data, by studying the envelope of the signal. It is very easy to show if there is some field induced effect, the magnitude of magnetic fields that give enhanced relaxation and if the effect occurs in the whole of the sample or in just some fraction of the volume.

We extended our study in Expts. 918 and 950 to other samples, trying to determine a correlation between the parent compound, doping with Eu or Zn and the increased relaxation rate. In the case of $\text{YBCO}(\text{Zn}0.7\%)$ we found no field induced effect (Fig. 136). The relaxation rate is almost field independent, with a slow decrease as the external field increases. So far we found that increased relaxation occurs only in La_2CuO_4 based samples. In the case of the Europium doped LSCO, the effect is enhanced (Fig. 137). One interesting thing to note is the fact that we see an

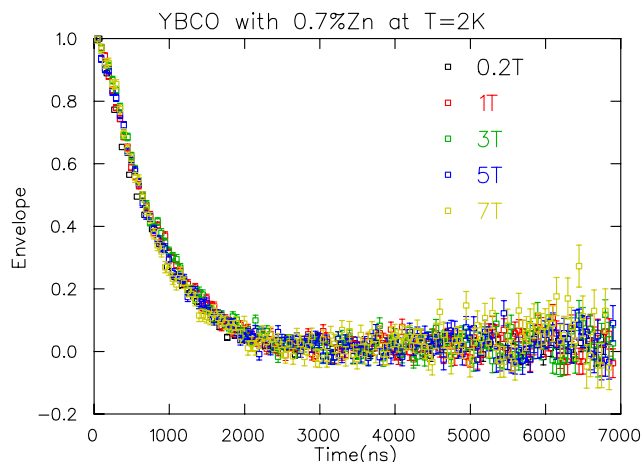


Fig. 136. Envelope functions at different magnetic fields for $\text{YBCO}(\text{Zn}0.7\%)$.

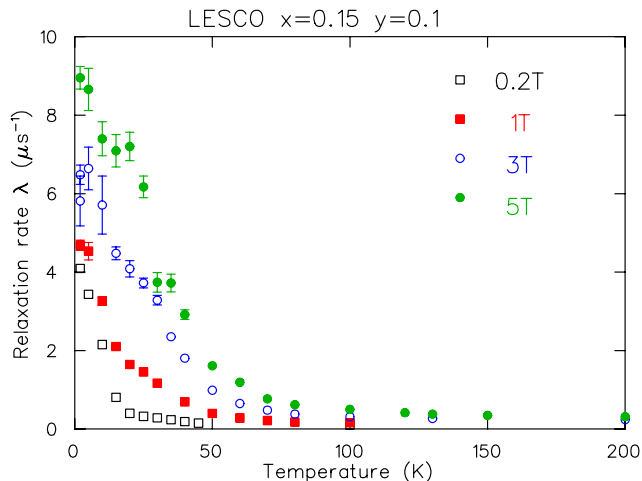


Fig. 137. Relaxation rates for exponential fits to TF- μSR signal in LESCO sample.

increased relaxation rate well above the superconductivity transition temperature.

Currently, we are working on determining the extent of the regions with induced magnetism.

Experiment 931

Magnetic properties of $\text{M}[\text{Au}(\text{CN})_2]_2 \cdot (\text{H}_2\text{O})_2$ ($\text{M} = \text{Cu}, \text{Ni}$) coordination polymers

(J.E. Sonier, D.B. Leznoff, SFU)

Introduction and background

Molecular magnetism deals with the magnetic properties of isolated molecules and groups of molecules, which contain one or more spin carriers. It is the combination of these spin carriers, the bridges connecting them, and their multidimensional assembly that generates materials with unique properties. At the heart of these investigations are two general goals: First, we seek to understand the magnetic interactions between spin carriers, both via direct bonding and mediated by ligand bridges. The key issue of interest is the strength and type of magnetic coupling (ferromagnetic or antiferromagnetic) for a given system. Second, methods to generate high-dimensional systems in a controlled fashion must be explored and applied to open-shell systems. Generally, high-dimensionality systems can show bulk properties (magnetic, thermal, optical) attributable to their polymeric nature. Metal-cyanide bridges have been extremely valuable in molecular magnetism research as they (a) readily form coordination polymers when reacted with transition-metal cations and (b) promote strong magnetic exchange. However, most studies have focused on octahedral $[\text{M}(\text{CN})_6]$ units. The Leznoff group has been exploring the use of linear cyanide units $[\text{M}(\text{CN})_2]$ ($\text{M} = \text{Ag}, \text{Au}$) as couplers in supramolecular open-shell systems. Dicyanoaurate and dicyanoargentate are unique

cyanometallates in that they are linear, form strong attractive M-M intermolecular interactions, and are luminescent.

Under Expt. 931 we have been examining the magnetic properties of some of Leznoff's multidimensional $[\text{Au}(\text{CN})_2]$ -containing coordination polymers that also incorporate paramagnetic transition-metal centres. In particular, the $\text{Cu}[\text{Au}(\text{CN})_2]_2 \cdot (\text{H}_2\text{O})_2$ system was shown in previous μSR studies to undergo a magnetic ordering transition at 250 mK. The questions we wished to probe included: (1) the nature of the magnetic exchange pathway in $\text{Cu}[\text{Au}(\text{CN})_2]_2 \cdot (\text{H}_2\text{O})_2$, i.e., whether the gold-cyanide unit or the copper-bound water molecules mediated the ordering phenomenon and (2) the effect of altering the paramagnetic metal spin carrier on the magnetic properties.

$\text{Ni}[\text{Au}(\text{CN})_2]_2 \cdot (\text{H}_2\text{O})_2$ was prepared and shown to have a very similar structure to the copper analogue. By using SQUID magnetometry between 2–300 K it was determined that this compound undergoes a magnetic phase transition at a much higher temperature than the copper analogue, but with complicated magnetic field-dependent behaviour. Field-dependent dc and ac measurements were conducted and a μSR investigation of this material was desired in order to aid the understanding of the magnetic phase diagram. The results are reported below. The results of these experiments are expected to be submitted for publication in the near future.

Both compounds examined by μSR have been characterized with a variety of other techniques (IR, elemental analysis, TGA etc.) but unfortunately, their structures have not been determined by single-crystal X-ray diffraction, although we are attempting to gain some structural information from powder diffraction data.

$\text{Cu}[\text{Au}(\text{CN})_2]_2 \cdot (\text{H}_2\text{O})_2$

To address the issue of the magnetic pathway in this material, the anhydrous copper/gold material, $\text{Cu}[\text{Au}(\text{CN})_2]_2$, was prepared. If the magnetic exchange interaction leading to ordering is via the metal-bonded water molecules via intermolecular hydrogen bonding, then the removal of these water molecules ought to greatly impact the ordering behaviour. If, however, the gold atoms are primarily responsible, then the ordering behaviour should persist.

We performed zero-field μSR on the anhydrous compound and found no evidence of magnetic order at temperatures down to 50 mK, as is evidenced by the lack of an oscillation in the time spectra presented in Fig. 138. In addition, the relaxation of the muon spin polarization at $T = 400$ mK was largely quenched in longitudinal fields as low as 200 G, indicating that the magnetic moments are primarily static in nature. The

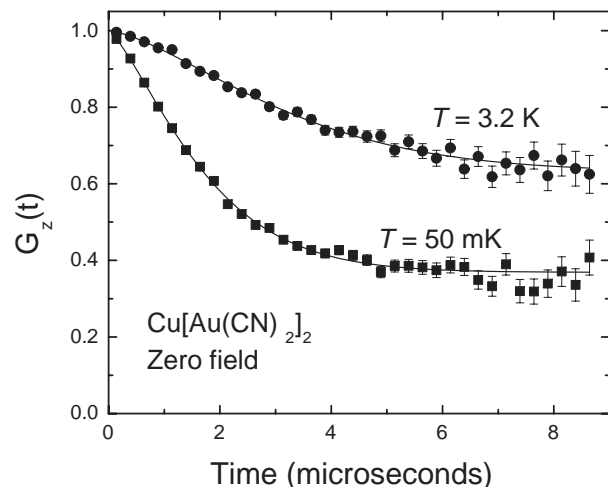


Fig. 138. Time-evolution of the muon spin polarization at various temperatures in $\text{Cu}[\text{Au}(\text{CN})_2]_2$.

lack of magnetic order is in stark contrast to the hydrated compound, and we can therefore conclude that the magnetic interaction in $\text{Cu}[\text{Au}(\text{CN})_2]_2 \cdot (\text{H}_2\text{O})_2$ is mediated by the metal-bonded water molecules.

$\text{Ni}[\text{Au}(\text{CN})_2]_2 \cdot (\text{H}_2\text{O})_2$

Zero-field μSR measurements as a function of temperature were performed on this material in an effort to determine the effect of altering the paramagnetic metal spin carrier on the magnetic properties. The zero-field time-evolution of the muon spin polarization at various temperatures is shown in Fig. 139. Figure 140 shows the corresponding relaxation rates extracted from fits of the time spectra to a stretched exponential function. It can be seen that the relaxation rate rises rapidly below $T \simeq 5$ K, indicating a slowing down of the fluctuations of the magnetic moments, but there is no indication of long-range magnetic order. This contrasts with $\text{Cu}[\text{Au}(\text{CN})_2]_2 \cdot (\text{H}_2\text{O})_2$ in which the spins freeze into an ordered state at the much lower temperature of 250 mK.

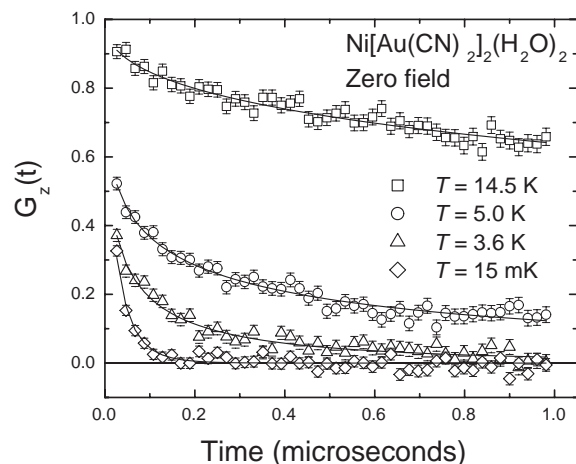


Fig. 139. Time-evolution of the muon spin polarization at various temperatures in $\text{Ni}[\text{Au}(\text{CN})_2]_2 \cdot (\text{H}_2\text{O})_2$.

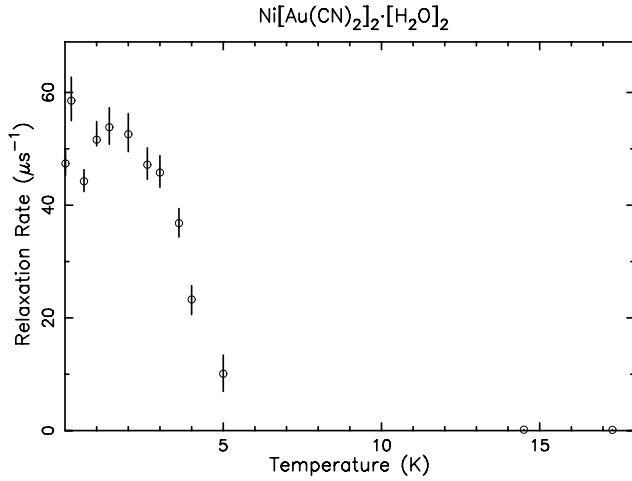


Fig. 140. Relaxation rate of the muon spin polarization as a function of temperature in $\text{Ni}[\text{Au}(\text{CN})_2]_2 \cdot (\text{H}_2\text{O})_2$.

Experiment 938

Muonium formation and ionization in semiconductors and insulators

(V.G. Storchak, Kurchatov; J.H. Brewer, UBC-TRIUMF)

Deep muonium in InSb

The exquisite time resolution and high magnetic field capabilities of TRIUMF's HiTime μSR spectrometer have facilitated the first direct observation of a muonium ($\text{Mu} = \mu^+ e^-$) bound state in indium antimonide. Figure 141 shows the characteristic field dependence of the three detectable frequencies (diamagnetic, ν_{12} and ν_{34}). Frequencies as high as 2.5 GHz have been observed in the HiTime spectrometer, whose true time resolution is estimated to be ~ 140 ps, but in this case the amplitude of the highest frequency signal was too small to follow above about 2 GHz.

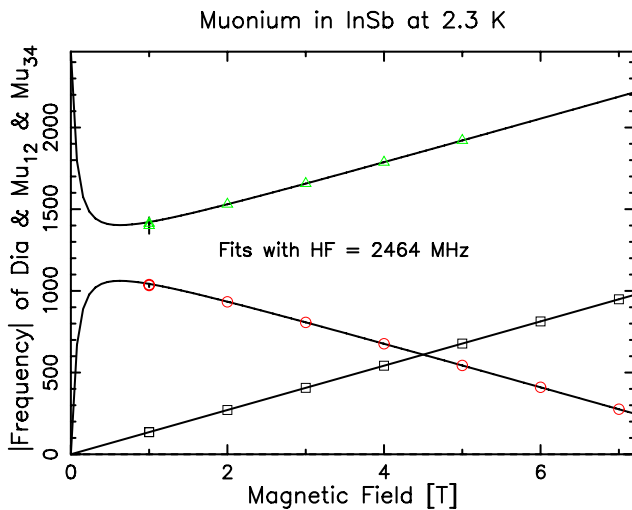


Fig. 141. Frequencies of diamagnetic (squares) and muonium (circles and triangles) precession signals in InSb at 2.3 K as functions of applied magnetic field.

The small-amplitude Mu signal was characteristic of “deep” tetrahedral muonium (Mu_T); there was no sign of the bond-centred Mu_BC state that has been so ubiquitous in other semiconductors [Patterson, Rev. Mod. Phys. **60**, 69 (1988)], nor was there any hint of the metastable “shallow” (weakly bound) Mu_WB state [Shimomura *et al.*, Phys. Rev. Lett. **89**, 255505.1 (2002); Eshchenko *et al.*, Physica **B326**, 120 (2003)] that was expected (given the high mobility and low effective mass of electrons in InSb).

However, there is a substantial “missing fraction” of muon polarization. Either Mu_BC or the shallow Mu_WB state may show up in subsequent experiments at dilution refrigerator temperatures.

The fractions of muon polarization shown in Figs. 142 and 143 have been corrected for the finite

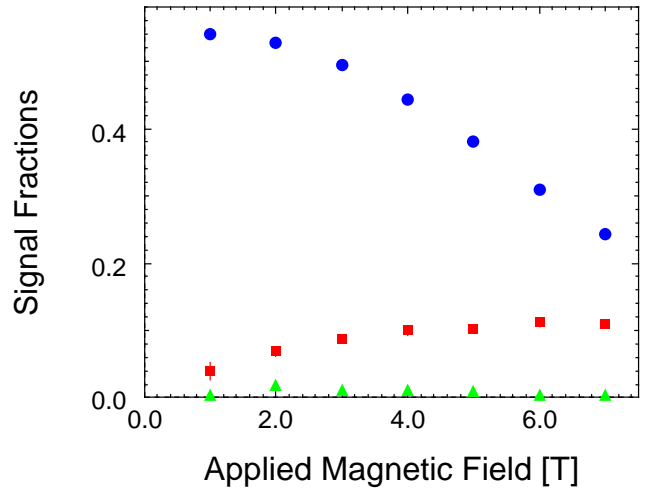


Fig. 142. Magnetic field dependence of diamagnetic (circles) and muonium (squares and triangles) signal amplitudes (expressed as fractions of the maximum muon decay asymmetry) in InSb at 2.3 K.

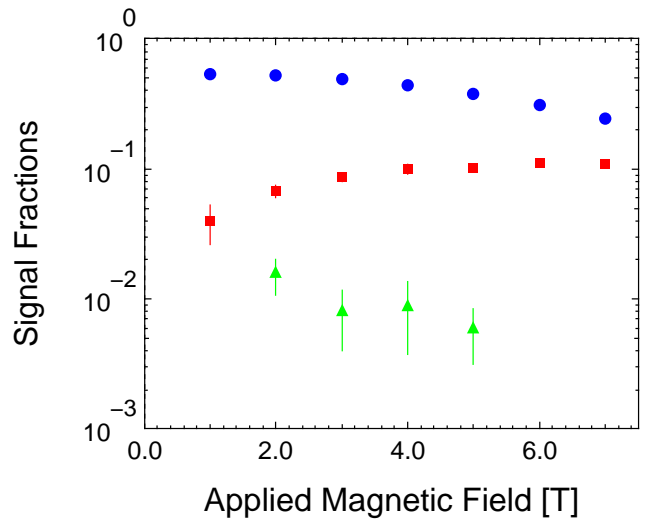


Fig. 143. Same as Fig. 142 except that the signal amplitudes are shown on a logarithmic scale.

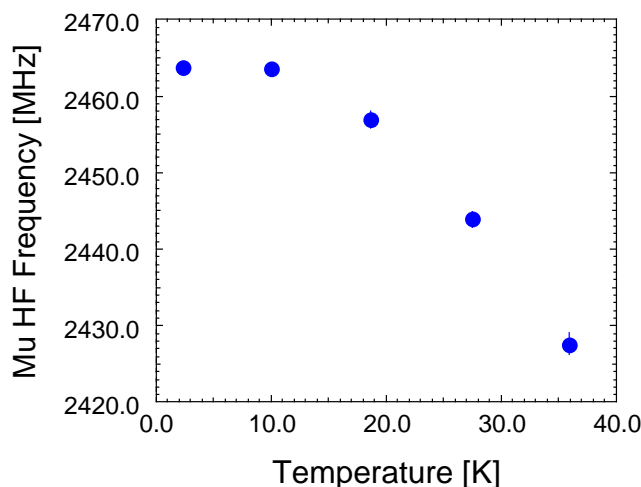


Fig. 144. Temperature dependence of the fitted hyperfine frequency of the deep muonium state in InSb.

time resolution of the HiTime spectrometer by dividing by the value at the same frequency of a smooth function fitted to the measured field dependence of the amplitude of a silver reference sample. The increase of the muonium fraction with field at the expense of the diamagnetic fraction is therefore a real phenomenon, and not a systematic effect. This is thought to reflect magnetic freezeout of radiolysis electrons into a weakly bound excited precursor state, as seen in GaAs [Storchak *et al.*, submitted to Phys. Rev. Lett.].

As can be seen from Fig. 144, the muonium hyperfine frequency was strongly temperature dependent, as seen in previous experiments in high magnetic field [Kiefl *et al.*, Phys. Rev. Lett. **53**, 90 (1984)].

Experiment 939

Guest-host interactions and Hfcs of Mu-alkyl radicals in zeolites

(D.G. Fleming, UBC)

In continuation of Expt. 939 as described in the 2002 Annual Report, the guest-host interactions and Hfcs of the Mu-ethyl radical were studied in the HY and USY zeolites, at 1 and 5 per supercage (SC) and 1 per SC, respectively. For details on experimental plans, loading techniques and terminologies please see that report. As seen in Fig. 145, differences in muon-hyperfine coupling constants (Hfcs) of Mu-ethyl in HY due to different loadings are quite small, differing by no more than 6%, suggesting that radical interactions with other guest molecules in the zeolite are negligible. Consistent with our previous data, however, cation-type effects on hyperfine coupling (due to zeolite type) are quite large, yielding an increase in Mu-Hfc of ~15% between HY and NaY. Unexpectedly, there was very little difference in the magnitude of Hfcs seen in HY and USY (a ~100% cation free zeolite), although the shapes of the temperature-dependence curves showed

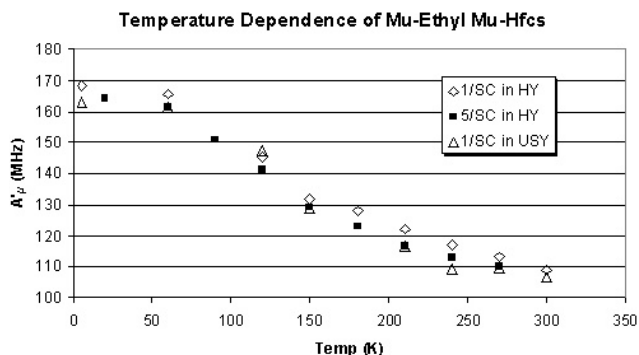


Fig. 145. Muon Hfcs for the Mu-ethyl radical in the HY (at 1 and 5 per supercage loadings) and USY (at 1 per supercage) zeolites. Note that it is the reduced muon Hfc, $A'_{\mu} = A_{\mu}/3.184$, that is plotted. It is also noteworthy that very little loading dependence exists in HY, and that radicals in the USY zeolite show a different T-dependence than those in the HY zeolite.

different curvatures at the inflection points and at low temperatures. USY shows a sharper inflection point than seen in HY suggesting two (or more) sterically-frozen orientations in the former case, a transition between which requiring overcoming a relatively large activation energy barrier. The McConnell plateau (at low temperatures, the y-intercept of which represents the Hfc of a molecule in the absence of internal rotation at 0 K) for the USY-bound radical is flatter, also supporting this idea. Alpha- and Beta-proton Hfcs (not shown in figure) were not well observed in USY, but in HY were shown to have a significant loading- and temperature-dependence, differing by 10–15% when compared at 1 and 5 per SC, and increasing by 10 MHz (15%) when the temperature was increased from 150 to 300 K.

In 2003, the only requirement for completion of the Mu-t-butyl study in Expt. 939 was to investigate the possible formation of the Mu-isobutyl radical in parallel with Mu-t-butyl. This radical is not easily observed, and it is thought rarely forms (by a pseudo-*anti*-Markovnikovian argument), but previous data from 2002 showed its potential presence in an LCR spectra at 240 K. High-statistics TF and ALCR tests were both performed on isobutene-loaded NaY at and around 240 K, showing the presence of no such radical. With the extra time available this summer, 2-cis-butene, 2-trans-butene, and 1-butene were surveyed in NaY and HY. Bulk 2-cis-butene was also investigated thoroughly, the results of which will be reported completely following Expt. 939's summer 2004 beam time. Figure 146 shows the preliminary results of the "butenes" study in zeolites. As is evident, there is little difference between the Mu-Hfcs from the addition of muonium to 2-cis-butene (studied from 7–320 K) and 2-trans-butene (only probed at 300 K). This is to be expected, as the radical yielded in both cases is

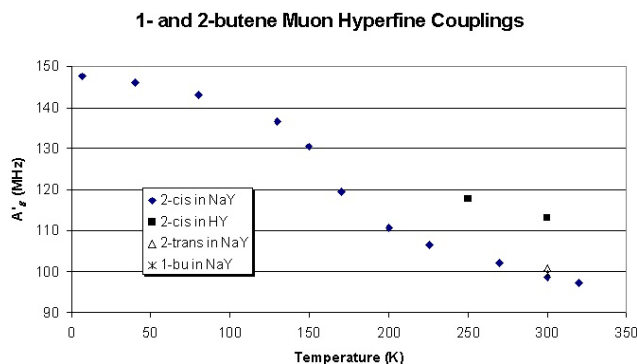


Fig. 146. Muon Hfcs for the Mu-butyl radical (from 2-cis-, 2-trans-, and 1-butene) in the NaY and HY zeolites at 2 per SC loadings. Again, it is A'_μ that is plotted. Note the significant dependence on cation type.

the Mu-butyl radical ($\text{CH}_3\text{CH}\cdot\text{CHMuCH}_3$). Addition of muonium to 1-butene also yields Mu-butyl, but of the form $\text{CH}_2\text{MuCH}\cdot\text{CH}_2\text{CH}_3$, which should yield different hyperfine coupling behaviour. At room temperature, all three butene-types in NaY yielded similar Hfcs; if this holds true at lower temperatures it has yet to be seen. The best potential for future investigation lies in the study of Hfc-dependence on cation type for 2-cis-butene (as is shown to be substantial at room temperature in the figure), and for 1-butene, which should yield some interesting differences from the former molecule. It is our intention to wrap-up the experimental project this summer.

Experiment 941

Investigation of spin statics and dynamics in the transition metal oxides $\text{Sr}_2\text{CaReO}_6$ and $\text{Li}_2\text{Mn}_2\text{O}_4$

(C.R. Wiebe, Columbia/McMaster; G.M. Luke, McMaster)

The topic of geometric frustration has been at the forefront of solid state physics for the last decade due to the remarkable number of interesting magnetic ground states observed. The plethora of lattice types which can accommodate the triangular motif of spins coupled with the arsenal of magnetic species to place on these sites has brought about a unique subfield of magnetism that will remain to be studied for a long time. In the last few years, the focus of study has shifted to the search for more exotic systems such as the spin liquid, which arises due to quantum effects from networks of frustrated low spin materials. For example, the pyrochlore $\text{Tb}_2\text{Ti}_2\text{O}_7$ has recently been shown to be a “cooperative paramagnet”, in which the system shows no magnetic long range order down to 0 K but instead forms a liquid like state. Neutron diffraction and μSR experiments were crucial in the elucidation of the important role of strong spin fluctuations that persist down to 0 K. Such discoveries provide the im-

petus to look for new materials that will continue to challenge and surprise the condensed matter community.

Despite this high level of interest, the number of examples of frustrated systems with isolated low-spin moments is relatively small. Spin liquids have proven to be difficult subjects of study with the exception of a few well known materials. The number of systems that display little disorder and have well-defined low spins on frustrated topologies is relatively low.

Spin freezing in the ordered FCC perovskite $\text{Sr}_2\text{CaReO}_6$

Two new materials have recently been synthesized at the Brockhouse Institute for Materials Research that are excellent candidates for displaying liquid-like ground states. $\text{Sr}_2\text{CaReO}_6$ is an FCC perovskite that has an ordered array of FCC $S = 1/2 \text{ Re}^{6+}$ moments. These form a network of edge-shared tetrahedra as displayed in Fig. 147. A FC/ZFC divergence in the DC susceptibility suggests a transition at 14 K. Neutron diffraction experiments failed to detect any long range ordering below this temperature. Recent heat capacity measurements hint at the presence of interesting spin dynamics at play through the appearance of an anomaly at T_G that is independent of the applied magnetic field. This is reminiscent of a spin singlet ground state, as suggested by Ramirez *et al.* from his work on the kagomé material $\text{SrCr}_{9p}\text{Ga}_{12-9p}\text{O}_{19}$ (SCGO). Furthermore, the magnetic specific heat shows a T^3 dependence at low temperatures, which suggests that strong 3D spin fluctuations are present as $T \rightarrow 0 \text{ K}$. Similar behaviour is seen in SCGO, with a T^2 specific heat power law, indicative of 2D spin fluctuations that were later confirmed by μSR measurements.

μSR has long been used to study the dynamics of highly frustrated spin systems. For small S spin systems in particular, muons are perhaps the best probe of the low temperature magnetic ground state within a broad frequency range. Figure 148 shows several zero

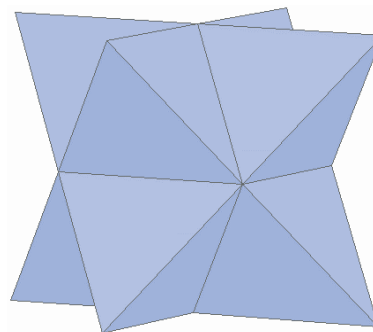


Fig. 147. The face-centred cubic lattice of Re^{6+} spins in $\text{Sr}_2\text{CaReO}_6$, which can be envisioned as a sublattice of edge-shared tetrahedra.

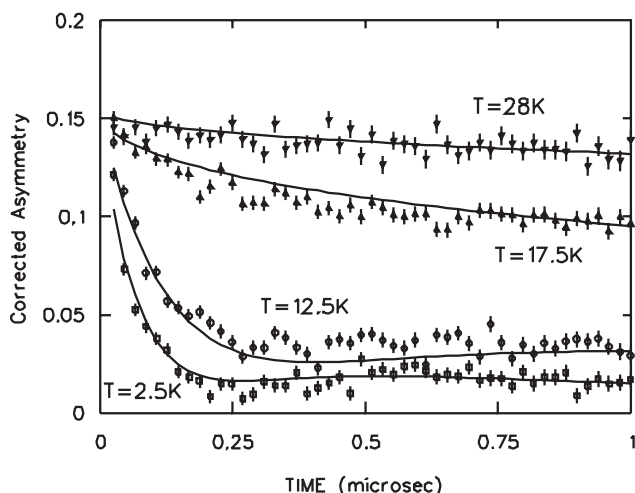


Fig. 148. ZF- μ SR measurements of $\text{Sr}_2\text{CaReO}_6$ at $T = 2.5$ K, 12.5 K, 17.5 K, and 28 K. The fits are based upon a generic spin glass relaxation function as described in the text.

field (ZF) scans taken between $T = 2.5$ K and $T = 28$ K. The two component nature of the spectra is immediately evident below $T_G \sim 14$ K, as opposed to the single component high temperature scans which is characteristic of a paramagnetic response. This response indicates a quasi-static distribution of internal magnetic fields developing below T_G , as noted in other spin glasses. The fit to the spectra indicated is modelled after Uemura's original treatment of these line-shapes in his pioneering μ SR work on AuFe and CuMn alloys. This is unusual with the absence of chemical disorder.

Although it seems like this system is a typical spin glass from the μ SR measurements, there are several departures from convention which merit further discussion. Firstly, the signal is somewhat weak, which is expected due to the small magnetic moment, but since it is feeble, it is truly difficult to tell if there is a weak ordering signal buried in the background. There could indeed be short ranged magnetically ordered clusters forming that are virtually undetectable by this technique. One would expect spin fluctuations at temperatures slightly higher than T_G to be visible in the spectra, but the nature of the transition itself is rather abrupt, with only the slightest hint of a second component appearing at $T = 17.5$ K. It is surprising that the second component develops quickly below T_G . The conventional way of understanding spin glasses is in the formation of islands of frozen spins which slowly develop as one passes through the transition. In our system, however, there is relatively little change in the muon signal from 12.5 K to 2.5 K, which suggests that the spins freeze out rather abruptly.

One can compare these results with the monoclinic $S = 1$ FCC ordered system $\text{Sr}_2\text{NiTeO}_6$ which shows a

lambda anomaly at $T_N \sim 28$ K indicative of magnetic ordering and a continuous phase transition. Nonetheless, magnetic susceptibility measurements show evidence for magnetic correlations at $T \sim 35$ K by a FC/ZFC divergence at temperatures higher than the cusp at T_N . In this case, approximately 70% of the entropy is recovered at the magnetic transition, but the ground state is ordered rather than glassy. As the Ni^{2+} ions in $\text{Sr}_2\text{NiTeO}_6$ have $S = 1$, this seems to suggest that it is the $S = 1/2$ moment on Re^{6+} that induces the spin glass ground state in $\text{Sr}_2\text{CaReO}_6$. This new ground state is believed to be caused by quantum effects of $S = 1/2$ spins on this highly frustrated lattice.

2D magnetic ordering in the 3D frustrated spinel $\text{Li}_2\text{Mn}_2\text{O}_4$

The other material of interest is the tetragonal spinel $\text{Li}_2\text{Mn}_2\text{O}_4$. This member is part of a series of materials, $\text{Li}_x\text{Mn}_2\text{O}_4$ ($x = 0-2$), which have been intensely studied as cathodes for secondary lithium ion batteries. All of these materials are in principle frustrated, since the Mn cations form a framework of corner-shared tetrahedra within the spinel structure (see Fig. 149). However, it is only the materials of low lithium content, such as $\lambda\text{-MnO}_2$ and LiMn_2O_4 that have been studied a great deal, due to interest by the electrochemical community. The fully lithiated species is difficult to synthesize without disrupting the structure unless one uses gentler methods, such as chimie douce. Insertion of Li by the addition of butyl-lithium to LiMn_2O_4 in an inert argon environment has been shown to be a successful method by our group to obtain the metastable $\text{Li}_2\text{Mn}_2\text{O}_4$ with only modest heating to 50°C .

$\text{Li}_2\text{Mn}_2\text{O}_4$ consists of a network of Mn^{3+} moments upon a lattice of slightly distorted corner-shared tetrahedra. Recently, Wills *et al.* have demonstrated that

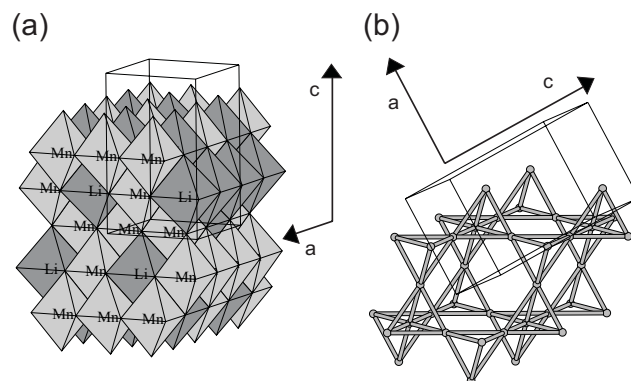


Fig. 149. (a) The spinel lattice, with Li and Mn octahedra. The a and c axis and the tetragonal unit cell are shown. (b) The Mn magnetic sublattice, shown as a network of corner-shared tetrahedra (which would be identical to the cubic pyrochlore sublattice if not for the tetragonal distortion). This can be thought of as a series of kagomé slabs normal to the $\langle 111 \rangle$ direction.

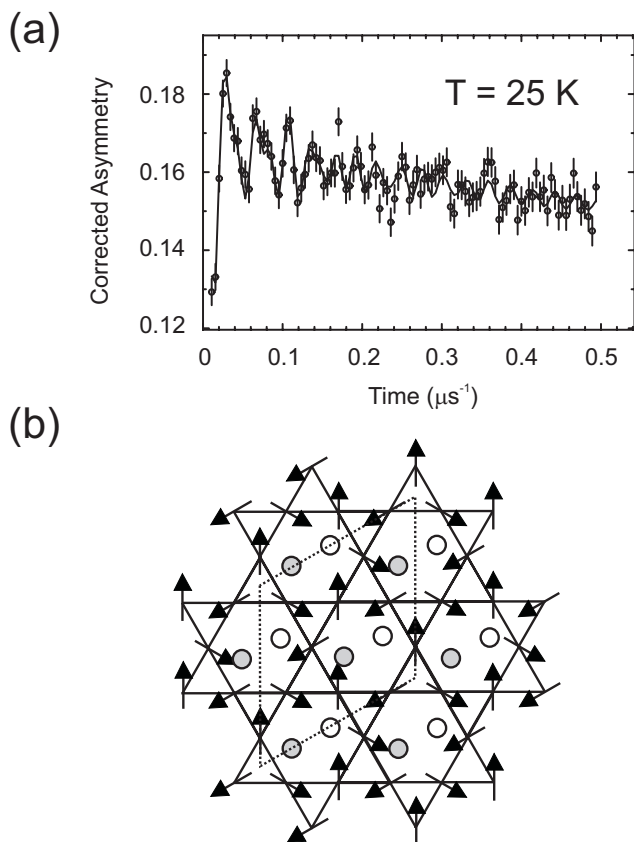


Fig. 150. (a) Early time ZF- μ SR spectra at $T = 25\text{ K}$. The fit is to a three frequency model. (b) The $q = \sqrt{3} \times \sqrt{3}$ magnetic structure. The muon sites in $\text{Li}_2\text{Mn}_2\text{O}_4$ are indicated on the figures as circles, slightly above (grey) and below (white) the kagomé planes. The magnetic sublattice in 2D is marked by dashed lines. There are six muon sites for the $q = \sqrt{3} \times \sqrt{3}$ structure, which give rise to the three frequency signal.

the frustrated lattice does not exhibit long-range order, but instead there is a transition to a short-range ordered state at 50 K . This is heralded by the appearance of several broad features in the elastic neutron scattering profile that can be fit to a Warren lineshape. As Warren indicated in his studies of graphite, these features are due to 2D correlations which arise in powder samples. In our case, the diffuse scattering is magnetic rather than structural, indicating strong 2D magnetic correlations. This is remarkable considering the fact that the connectivity of the frustrated lattice is fully three dimensional.

ZF- μ SR experiments on $\text{Li}_2\text{Mn}_2\text{O}_4$ have confirmed that a short-ranged ordered magnetic state sets in below $\sim 150\text{ K}$, which subsequently develops into a long-ranged ordered state below $\sim 50\text{ K}$. Longitudinal field measurements show that the fast relaxation seen in the regime $50\text{ K} \leq T \leq 150\text{ K}$ is static in nature, which is consistent with the broad features seen by neutron scattering. The ordering observed below 50 K

is compatible with the proposed two-dimensional $q = \sqrt{3} \times \sqrt{3}$ magnetic structure in kagomé planes that reside within the pyrochlore framework (see Fig. 150). The evolution of the order parameter at T_N resembles other 2D magnetic systems, but it is unclear why a three-dimensional network of tetrahedra would exhibit two-dimensional magnetism.

Experiment 943

Muonium formation and reactivity in sub- and supercritical carbon dioxide

(K. Ghandi, UBC)

Current data on muonium chemistry in supercritical water (Expt. 713/842) have established that the current models used in reaction kinetics of chemical reactions in supercritical water are wrong and they have led to a new model for chemical kinetics in supercritical water [Ghandi and Percival, J. Phys. Chem. **A107**, 3005 (2003); Ghandi *et al.*, Physica **B326** 76 (2003); Ghandi *et al.*, Phys. Chem. Chem. Phys. **4** 586 (2002); Ghandi *et al.*, Physica **B289**, 476 (1999)]. They have also led to novel mechanistic information relevant to green chemistry [Ghandi *et al.*, JACS **125**, 9594 (2003)]. In an attempt to extend those kinds of studies to supercritical CO_2 , we initiated Expt. 943.

The main focus of the first year of the experiment was to establish muonium formation over a broad range of thermodynamic states under sub-and supercritical conditions. In Figs. 151–153 we have compared our data with those in supercritical water [Percival *et al.*, Phys. Chem. Chem. Phys. **1**, 4999 (1999)] in a similar range of density and in high-pressure ethane [Kemp-ton *et al.*, J. Phys. Chem. **95**, 7338 (1991)] over a much smaller range of density. The comparison reveals significant difference in the radiolysis processes in supercritical CO_2 as compared to the other two fluids [Ghandi *et al.* (submitted to J. Phys. Chem. B)]. This may suggest that kinetics and interactions of thermal muonium

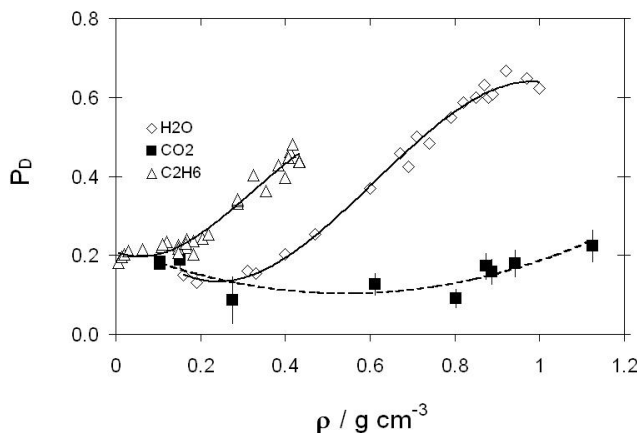


Fig. 151. Diamagnetic (P_D) fractions in pure CO_2 , H_2O and C_2H_6 as a function of density (error bars for C_2H_6 and H_2O data are not shown). The lines are to guide the eye.

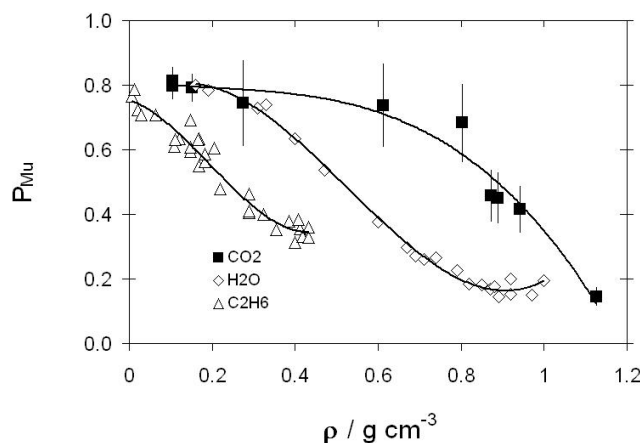


Fig. 152. Muonium (P_{Mu}) fractions in pure CO_2 , H_2O and C_2H_6 as a function of density (error bars for C_2H_6 and H_2O data are not shown). The lines are to guide the eye.

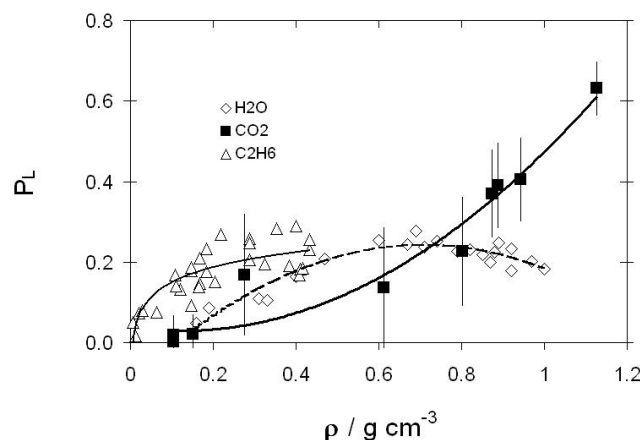


Fig. 153. Loss fractions (P_L) in pure CO_2 , H_2O and C_2H_6 as a function of density (error bars for C_2H_6 and H_2O data are not shown). The lines are to guide the eye.

are expected to be different compared to ones in supercritical water. To probe the change of interactions of Mu with solvent molecules (CO_2) with varying density, we have studied muonium hyperfine interactions at different densities. Our results, which are the subject of another publication, are shown in Fig. 154. This is the first demonstration, by any technique, of the effect of thermodynamic conditions in supercritical CO_2 on the atomic wave functions, and of a manifestation of change in intermolecular interactions between CO_2 and Mu. The data cover a much broader density range compared to the supercritical water data.

Also to extend the kinetic studies in supercritical water to supercritical CO_2 , we studied the reaction between NO and Mu. The rate of Mu decay is a result of two processes: spin exchange and addition of Mu to NO. Some early results are shown in Figs. 155 and 156 by using the $\frac{3}{4}$ law predicted by Senba [J. Phys. **B26**, 3213 (1993)] to separate the spin exchange from the additional component.

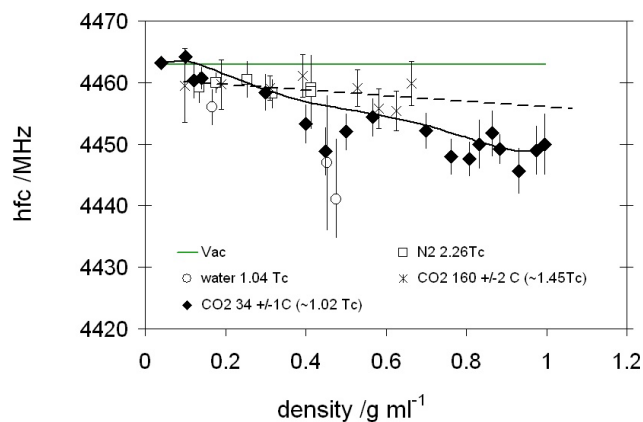


Fig. 154. Mu hyperfine coupling constant in supercritical CO_2 compared to in N_2 and in water.

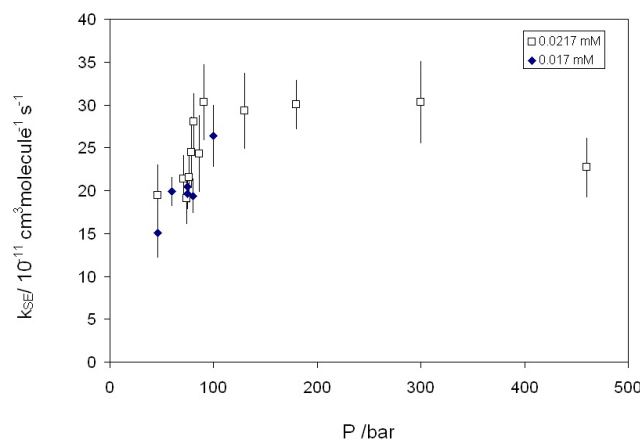


Fig. 155. The rate constant for spin exchange of Mu and NO at slightly above the critical temperature of CO_2 .

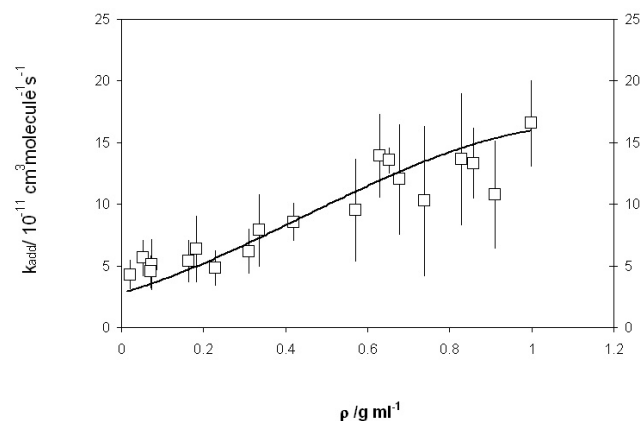


Fig. 156. The rate constant for the addition reaction of Mu and NO at slightly above the critical temperature of CO_2 .

The data on spin exchange may suggest a change in the diffusional and solvent cage properties in near critical CO_2 as observed for spin exchange between Mu and Ni^{2+} in supercritical water. The results for addition to NO show probably the first ever high-pressure limit for a reaction between Mu and a smaller than four atom molecule [Himmer *et al.*, J. Phys. Chem. **A103**,

2076 (1999); Pan *et al.*, Phys. Chem. Chem. Phys. **2**, 621 (2000)]. However, due to complications with addition to NO, more data, particularly in longitudinal field, are needed to confirm these results. It is intended to make such measurements over a wide density range at a few temperatures, with a view to separating the spin exchange from addition component by varying the magnetic field.

Experiment 944

Muonium in silicon carbide

(R.L. Lichti, Texas Tech; K.H. Chow, Alberta)

The main initial goal for TRIUMF Expt. 944 was to characterize the hyperfine interactions for neutral Mu centres seen in the three primary structures of SiC, namely 4H, 6H, and 3C. The cubic 3C structure was predicted to yield a shallow donor. We have not observed any Mu^0 hyperfine spectra in the *n*-type sample of 3C-SiC that was available, although features seen below 50 K suggest dynamics involving a possible shallow centre. Initial data for high-resistivity samples of the two hexagonal structures showed atomic-like neutral centres: two Mu^0 signals were observed in 4H as expected; and three strong Mu^0 signals were seen in 6H, but there were also hints of a possible fourth signal at some temperatures.

The three signals clearly observed in 6H-SiC do not correspond very well to the hyperfine values published some years ago [Patterson *et al.*, Hyp. Int. **32**, 625 (1986)]. The Mu^0 motion and related site averaging of A_{HF} that was expected to occur below 300 K based on the limited older data could not be confirmed. Instead we found that, although the precession signals of Mu^0 states disappeared between 100 and 200 K for the 6H sample, the same three signals reappeared at higher temperatures but below the onset of Mu^0 ionization near room temperature. Our main effort during this year's beam time was to examine *n*-type and *p*-type SiC to check for consistency in A_{HF} and to further characterize the unexpected Mu^0 dynamics.

In *n*-type 6H-SiC, two of the Mu^0 centres observed correspond to those seen in the high-resistivity material, but the third signal was significantly different, appearing in the region where hints of a possible fourth Mu^0 signal were seen previously. Table XII gives the zero temperature A_{\parallel} values in all 4H and 6H samples. We note that the values we find for *n*-type 6H are each about 20 MHz lower than the A_{\perp} values from the early results.

Figure 157 displays the temperature dependent hyperfine constants for one of the Mu^0 centres in 4H-SiC. The same two neutrals were seen in all 4H samples examined, and the data in Fig. 157 show typical

Table XII. The low-temperature hyperfine constants A_{\parallel} (in MHz) for Mu^0 centres observed with $\mathbf{B} = 6 \text{ T} \parallel \mathbf{c}$ in the 4H and 6H structures of silicon carbide.

Sample	High-resist	<i>p</i> -type	<i>n</i> -type
4H-SiC	3002.82 (0.01)	3002.77 (0.01)	3002.8 (0.1)
	2801.14 (0.06)	2801.07 (0.04)	2801.0 (0.2)
6H-SiC	2999.01 (0.01)		
	2984.34 (0.01)		2981.3 (0.1)
			2777.9 (0.2)
	2745.57 (0.01)		2745.5 (0.1)

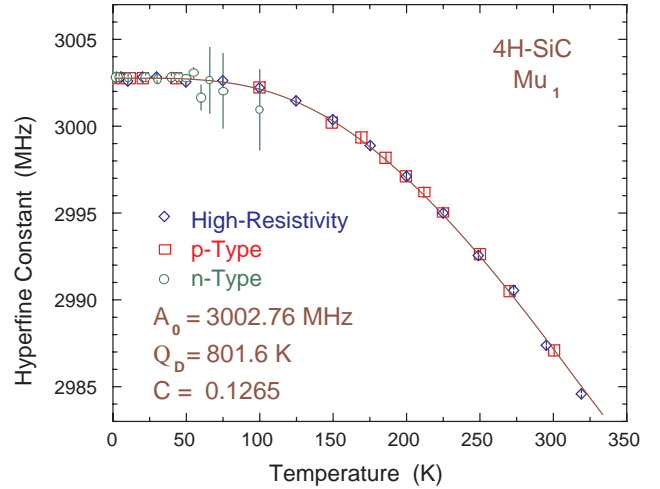


Fig. 157. Temperature dependent hyperfine constants for one of the two Mu^0 centres observed in 4H-SiC measured with $B = 6.0 \text{ T}$ applied along the *c*-axis.

sample to sample differences. For both *n*-type materials the Mu^0 spin precession signals broaden and disappear near 100 K where the nitrogen donors have ionized. The temperature dependence of A_{\parallel} fits well to a model in which the dominant cause of decreasing A_{HF} is interaction with long wavelength phonons. Each of the temperature-dependent A_{HF} curves in both 4H and 6H-SiC yields a Debye temperature of $\sim 800 \text{ K}$.

Longitudinal relaxation data were collected for the two *n*-type hexagonal samples as an initial attempt to identify specific transition or charge-exchange dynamics. Figure 158 shows the rate constants for the more rapidly relaxing fraction in *n*-type 6H-SiC. The amplitude associated with the feature between 100 and 180 K decreases with temperature, thus this feature probably represents a charge-state transition involving a single Mu^0 state, perhaps an electron capture to yield Mu^- at one of the occupied sites. Spin precession data for high-resistivity samples of both 4H and 6H suggest two diamagnetic states with a very small difference in frequencies of about 20 kHz out of 813 MHz, and the low-field precession data imply a transition between two diamagnetic states near 100 K.

The relaxing amplitude stays relatively constant across the higher temperature peak in Fig. 158, but

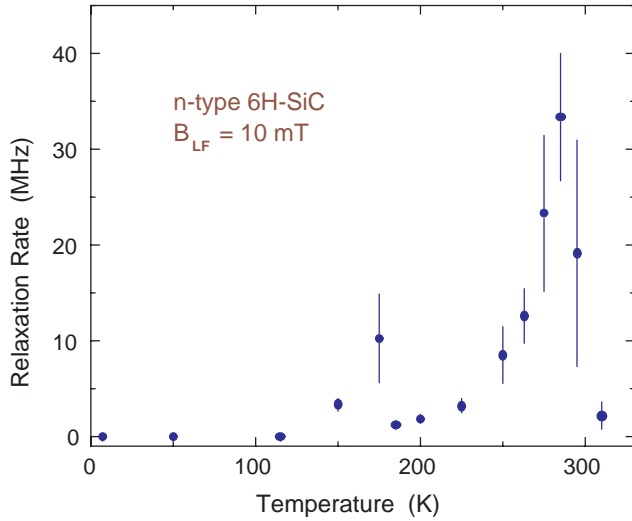


Fig. 158. Temperature dependence of longitudinal relaxation rates for the fast relaxing fraction seen in *n*-type 6H-SiC. Similar data for an *n*-type 4H-SiC sample show low rate constants and a sharp peak at 200 K.

then decreases above the peak. This is in the region where the spin precession data in *p*-type and high-resistivity samples imply an onset of Mu^0 ionization, thus we suggest a rapid $\text{Mu}^0 \leftrightarrow \text{Mu}^+$ charge-exchange cycle involving electron loss and recapture as the likely origin of this feature. These results show that a combination of spin precession and longitudinal relaxation data is beginning to provide hints of the origin of dynamics involving Mu^0 centres in hexagonal SiC.

Experiment 949

μSR study of magnetic order in high- T_c superconductors under high pressure

(J. Arai, Tokyo U. Science)

Anomalous suppression of superconducting transition temperature T_c observed in a narrow range of $x \sim 1/8$ for $\text{La}_{2-x}\text{M}_x\text{CuO}_4$ ($M = \text{Ba}, \text{Sr}$), which is called the “1/8 problem”, is one of the most important issues to understand the relation between superconductivity and magnetism in high- T_c cuprates. At the beginning, the 1/8 problem was considered to be particular to La-214 compounds. However, 1/8 anomaly is also observed in Bi-2212 and Y-123, suggesting that the 1/8 problem is a common property of high- T_c superconductors.

Structural instability is inherent in La-214 compounds, which are the most typical system in high- T_c superconductors. The crystal structure is closely related to the electronic state in this system. With decreasing temperature, La-214 compounds undergo a well-known phase transition from a high-temperature tetragonal (HTT) structure to a low-temperature orthorhombic (LTO) structure except for the overdoped region. In addition, $\text{La}_{2-x}\text{Ba}_x\text{CuO}_4$ (LBCO) displays

a second transition to a low-temperature tetragonal (LTT) structure around $x = 1/8$ at low temperatures. Because superconductivity is strongly suppressed in LBCO around $x = 0.125$ and slightly suppressed in $\text{La}_{2-x}\text{Sr}_x\text{CuO}_4$ (LSCO) around $x = 0.115$, it is widely believed that the LTT structure plays an important role in suppressing superconductivity around $x \sim 1/8$.

On the other hand, in La-214 compounds around $x \sim 1/8$, magnetic order has been observed by neutron scattering experiments [Tranquada *et al.*, Nature **375** (1995)] and μSR experiments [Watanabe *et al.*, J. Phys. Soc. Jpn. **61** (1992)]. These results indicate the close relation between the suppression of superconductivity and the appearance of magnetic order.

The μSR measurement is the most suitable experimental method to study the competition between superconductivity and magnetic order because we can investigate the Cu spin state in the absence of an external magnetic field. On the other hand, the LTT and LTO phases of LBCO with $x = 0.125$ are suppressed by applying pressure up to 0.6 GPa and 1.5 GPa, respectively [Katano *et al.*, Phys. Rev. **B48** (1993)]. Then we can control the two structural transition temperatures by applying pressure above 1.5 GPa.

To generate high pressure above 1.5 GPa, we have developed pressure cells made of non-magnetic alloy Ni-Co-Cr-Mo (MP35N) with a wall 8 mm thick. The size of the sample in the pressure cell is much smaller than that in conventional μSR measurements. To increase the SN ratio, we used the defining counter which is as small as the sample.

In order to clarify the relation among superconductivity, the magnetic order and the crystal structure, we have performed the zero-field μSR measurement in LBCO with $x = 1/8$ under high pressure up to ~ 1.3 GPa by using $\phi 7\text{T}8$ pressure cell at the M9B port at TRIUMF.

Figures 159 and 160 show the μSR spectra at ambient pressure and $P \sim 1.3$ GPa, respectively. Here we define the magnetic ordering temperature T_m as the temperature where an oscillation component starts to appear in μSR spectra. At ~ 1.3 GPa T_m exists between 35 and 40 K. The μSR spectra at 35 K under ambient pressure and ~ 1.3 GPa are quite similar. T_c at ambient pressure is the same as that at $P \sim 1.3$ GPa. Since the LTT structure vanishes above ~ 0.6 GPa, this result suggests that the magnetic order is not related to the LTT structure.

In order to investigate the relation between superconductivity and the LTT structure, we have carried out the resistivity measurement in LBCO with $x = 0.125$ at several pressures up to ~ 2.2 GPa. The superconducting temperature T_c which is determined by zero of the resistivity increases as the LTT structure

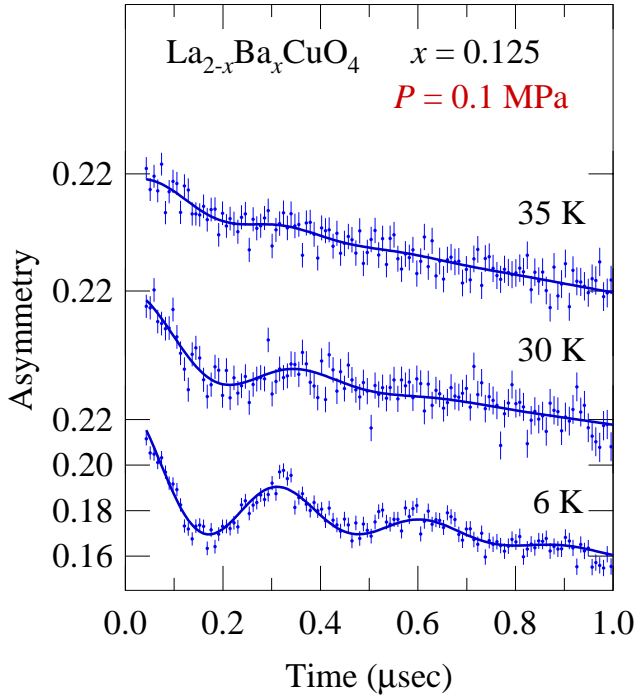


Fig. 159. ZF- μ SR spectra of LBCO with $x = 0.125$ at ambient pressure.

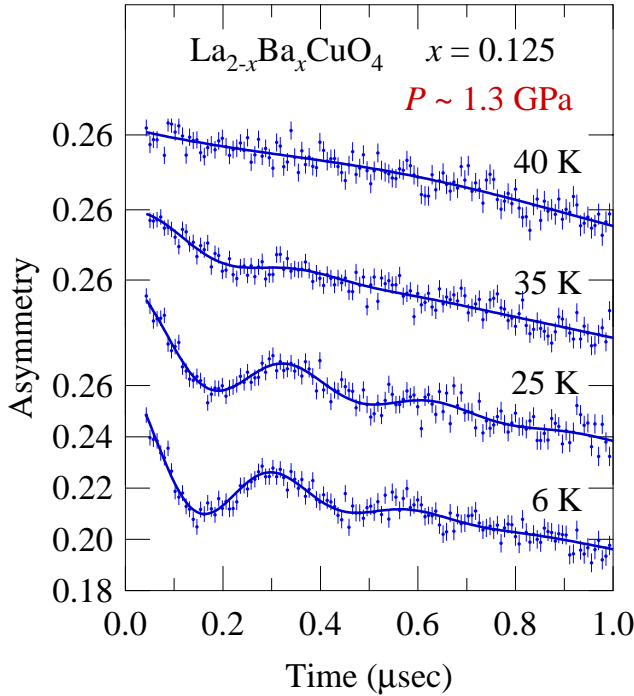


Fig. 160. ZF- μ SR spectra of LBCO with $x = 0.125$ at $P \sim 1.3$ GPa.

is suppressed. The suppression of superconductivity is closely related to the LTT structure.

T_m and T_c are plotted as a function of pressure in Fig. 161. With increasing pressure, T_c increases linearly with an initial rate of $dT_c/dP \sim +8.1$ K/GPa. At $P_d \sim 1.1$ GPa, dT_c/dP changes to $+1.9$ K/GPa.

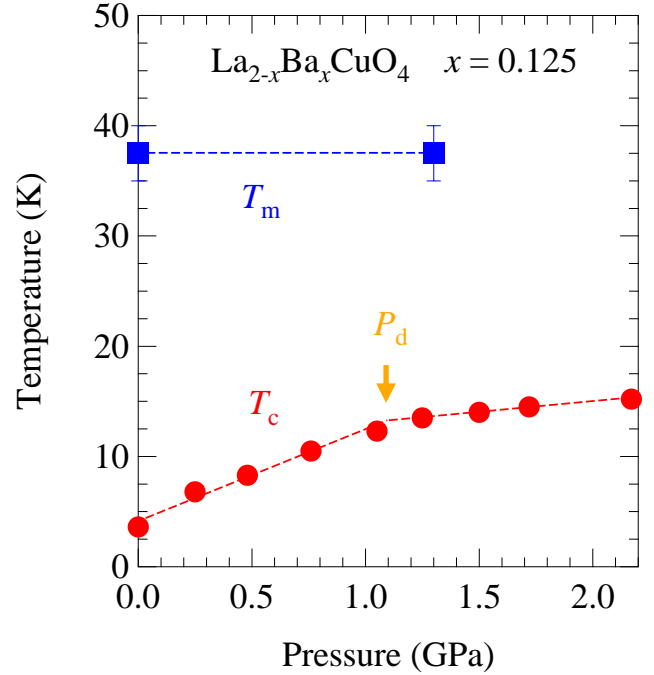


Fig. 161. Pressure dependence of magnetic ordering temperature T_m and superconducting temperature.

It seems that P_d indicates the LTT-LTO phase transition pressure. On the other hand, T_m is independent of pressure, suggesting that the magnetic order does not compete with superconductivity.

Experiment 951

Magnetism and flux line lattice structure of oxychloride superconductors

(K. Ohishi, R. Kadono, KEK-IMSS)

Alkaline-earth copper oxychlorides $A_2CuO_2Cl_2$ ($A = Ca, Sr$) are insulating antiferromagnetic compounds consisting of two-dimensional CuO_2 layers. They have a layered perovskite structure common to K_2NiF_4 with a body-centred-tetragonal symmetry ($I4/mmm$), which is free from any distortion. The Néel temperature (T_N) determined by neutron measurements is 255 K for $A = Sr$ [Vaknin *et al.*, Phys. Rev. **B41**, 1926 (1990)] and 247(5) K for $A = Ca$ [*ibid.*, Phys. Rev. **B56**, 8351 (1997)], respectively. While $Sr_2CuO_2Cl_2$ has yet to be carrier doped [Miller *et al.*, Phys. Rev. **B41**, 1921 (1990)], $Ca_2CuO_2Cl_2$ becomes a high- T_c superconductor (maximum $T_c = 28$ K at $x \sim 0.2$) by the doping of sodium [Hiroi *et al.*, Nature **371**, 139 (1994)]. While $Ca_{2-x}Na_xCuO_2Cl_2$ exhibits superconductivity upon doping holes by substituting Ca by Na, the magnetic property of those with $x < 0.10$ (which are non-superconducting) has not been investigated, except for $x = 0$. We have performed ZF- μ SR measurements to elucidate the magnetic phase diagram of $Ca_{2-x}Na_xCuO_2Cl_2$ over the underdoped region.

The ZF- μ SR measurements were conducted on the M15 beam line at TRIUMF. We prepared ten sets of $\text{Ca}_{2-x}\text{Na}_x\text{CuO}_2\text{Cl}_2$ specimens, $x = 0, 0.0025, 0.005, 0.01, 0.02, 0.05, 0.07, 0.10, 0.15, 0.20$, having a dimension of about $100 \sim 250 \text{ mm}^2$ with $\sim 1 \text{ mm}$ thickness. These samples were mounted on a sample holder and loaded to the ^4He gas flow cryostat. ZF- μ SR measurements were performed at temperatures between 2 K and room temperature, and transverse field (TF)- μ SR measurements were also performed at room temperature under applied field $H_{\text{TF}} \simeq 2 \text{ mT}$ in order to determine the geometrical factor. In this report, we show the result in $\text{Ca}_2\text{CuO}_2\text{Cl}_2$ ($x = 0$) for which the analysis is complete.

Figure 162 shows the time spectra of the muon spin polarization $P_z(t)$ observed in $\text{Ca}_2\text{CuO}_2\text{Cl}_2$ in zero field at several temperatures. The left and right figures show $P_z(t)$ over the respective time region of $7 \mu\text{s}$ and $1.0 \mu\text{s}$. For both time ranges, spin precessions with different frequencies are clearly observed below $T = 260 \text{ K}$. Therefore, μ SR data were analyzed with the following function;

$$P_z(t) = \sum_{i=1}^n A_i \exp[-(\sigma_i t)^2] \cos[2\pi(f_i t + \phi)] + A_{\text{non}} \exp[-(\sigma_{\text{non}} t)^\beta],$$

where A_i and A_{non} are the asymmetries of oscillating and non-oscillating components, f_i is the muon spin precession frequency, σ_i and σ_{non} are the relaxation rates, β is the power of the exponent.

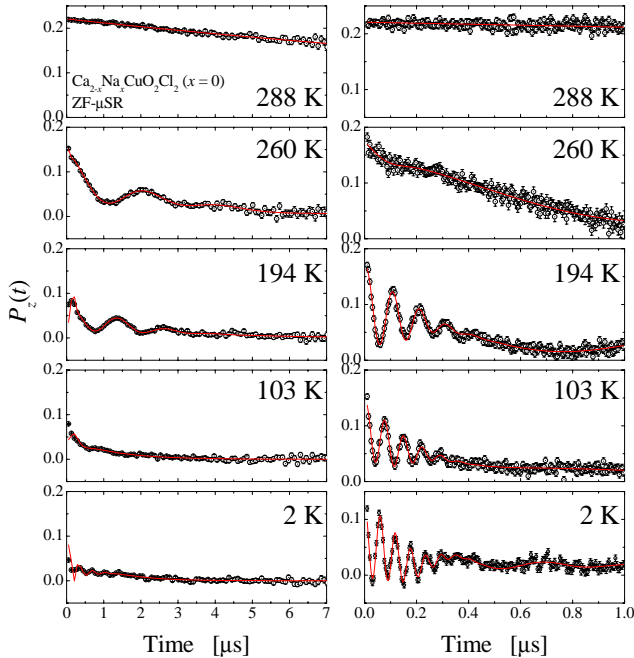


Fig. 162. ZF- μ SR time spectra of the muon spin polarization $P_z(t)$ in $\text{Ca}_2\text{CuO}_2\text{Cl}_2$ at various temperatures.

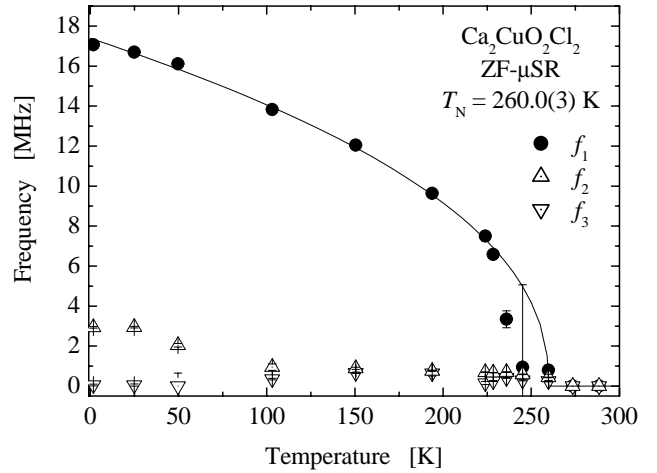


Fig. 163. Temperature dependence of the muon spin precession frequencies in $\text{Ca}_2\text{CuO}_2\text{Cl}_2$.

The temperature dependence of the muon spin precession frequencies is shown in Fig. 163. The frequencies are sharply reduced above 260 K, with their amplitudes disappearing around 275 K. This is consistent with the neutron results in which Bragg peak appears below $T_N = 247(5) \text{ K}$. It is also noticeable that one having lower frequencies further splits into two components below around 100 K. The high frequency component (f_1) is well fitted by a function $A(T_N - T)^B$, with $T_N = 260.0(3) \text{ K}$. This complex character of the internal field is in marked contrast with the case in $\text{La}_{2-x}\text{Sr}_x\text{CuO}_4$ where only a single frequency is observed. However, one of those (f_2) is almost the same as that in $\text{La}_{2-x}\text{Sr}_x\text{CuO}_4$ ($\sim 5 \text{ MHz}$) [Uemura *et al.*, Phys. Rev. Lett. **59**, 1045 (1987); *ibid.*, Physica **C153-155**, 769 (1988); *ibid.*, Hyp. Int. **49**, 205 (1989)] and f_3 is close to that in $\text{Sr}_2\text{CuO}_2\text{Cl}_2$ [Le *et al.*, Phys. Rev. **B42**, 2182 (1990)].

While the detailed analysis is still in progress, these findings suggest that the muon stopping site may not be unique. It is currently speculated that the muon sites are both at around apical chlorine, which is common to the $\text{La}_{2-x}\text{Sr}_x\text{CuO}_4$ case, and near oxygens in CuO_2 planes.

Experiment 953

Spin dynamics and quantum coherence in molecular magnets

(Z. Salman, TRIUMF; R.F. Kiefl, TRIUMF/UBC)

Molecular magnets are molecules consisting of ions coupled by strong ferromagnetic or anti-ferromagnetic interaction; these molecules crystallize in a lattice where neighbouring molecules are very well separated. At temperatures lower than the magnetic coupling J between ions inside the molecule, the spins of the ions are locked to each other, and the molecular magnets

behave like noninteracting spins, all with the same total spin quantum number S . The energy difference between the ground spin state of the molecule and the next excited spin state is of the order of J , therefore at low temperatures only the ground spin state S is populated. This state is $2S+1$ times degenerate in first order approximation. However, at even lower temperatures the degeneracy can be removed by additional magneto-crystalline anisotropic interactions such as the uniaxial term DS_z^2 , or rhombic term $E(S_x^2 - S_y^2)$ etc. When the temperature is high enough, transitions between different spin states of the molecules are thermally activated, but when the temperature is much lower than the energy difference between spin states, the transitions between them are only possible through a quantum mechanical process.

The $\text{K}_6[\text{V}_{15}^{\text{IV}}\text{As}_6\text{O}_{42}(\text{H}_2\text{O})]\cdot 8\text{H}_2\text{O}$ complex known as V_{15} [Müller and Döring, *Angew. Chem. Int. Ed. Engl.* **27**, 157 (1991)] is made of a lattice of molecules with fifteen V^{IV} ions of spin $1/2$, placed in a quasi-spherical layered structure formed of a triangle, sandwiched by two hexagons (see Fig. 164). When the temperature is lower than ~ 100 K the two hexagons of the V ions form an $S = 0$ state, leaving the three V ions on the triangle with an effective Hamiltonian [Chiorescu *et al.*, *Phys. Rev. Lett.* **85**, 4807 (2000); Barbara *et al.*, *Prog. Theor. Phys. Supp.* **145**, 357 (2002)]

$$\mathcal{H}_0 = -J_0 (\vec{S}_1 \cdot \vec{S}_2 + \vec{S}_2 \cdot \vec{S}_3 + \vec{S}_3 \cdot \vec{S}_1) - g\mu_B \vec{H} \cdot \sum_{i=1}^3 \vec{S}_i$$

where \vec{S}_i are the spins of the three V ions and $J_0 \simeq -2.445$ K is the effective coupling between the spins. At temperatures lower than 500 mK the V_{15} molecules reside in their spin $S = 1/2$ ground state, with negligible dipolar interactions (few mK) between neighbouring molecules. The V_{15} molecules have no anisotropy barrier and a large tunneling splitting at zero field, $\Delta_0 \simeq 80$ mK.

At very low temperature (below 2 K) the spin ground state of the V_{15} system is with spin $1/2$. At temperatures much lower than 2 K only transitions

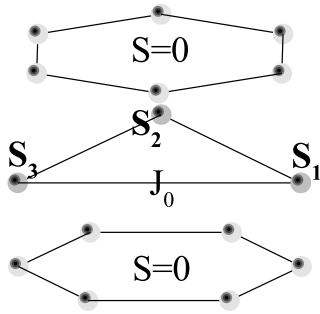


Fig. 164. The core of the V_{15} molecule. Only V ions are shown here.

between the $|+1/2\rangle$ and $|-1/2\rangle$ spin states are possible.

The muon spin lattice relaxation (SLR) rates, $1/T_1$, measured in V_{15} between 12 mK up to 300 K at various magnetic fields, are presented in Fig. 165. The high temperature SLR measurements show an increase in the SLR rates as the temperature is decreased due to the slowing down of the thermally activated transitions between the different spin states.

At $T \sim 100$ K a sudden increase in the SLR is observed at $H = 5$ G, a signature of the freezing of the V ions' spins on the hexagons (see Fig. 164), and the formation of $S = 0$ singlet state.

The relaxation rate at temperatures below ~ 10 K and at low fields (lower than 5 kG) becomes almost temperature independent, while at higher fields (5 and 10 kG) the relaxation rate decreases as the temperature is decreased down to 20 mK. At these temperatures mainly the $S = 1/2$ spin states are populated, and we attribute this decrease to the decrease in the thermally activated transitions between the $m = \pm 1/2$ states due to the Zeeman splitting. However, at even lower temperatures (less than ~ 200 mK) the SLR rate increases slightly, in agreement with ^1H NMR data [Yoneda *et al.*, *Physica* **B329-333**, 1176 (2003)].

The temperature dependence of the spin lattice relaxation at high temperatures indicates that the molecular spin dynamics at high temperatures is thermally activated. However, at low temperatures the spin dynamics is found to be temperature independent. This temperature independent behaviour is a strong indication that this spin dynamics is driven by the broadening and mixing of the spin states due to hyperfine interaction between the molecular and nuclear spins, and is the main contributor to the temperature independent spin lattice relaxation process observed.

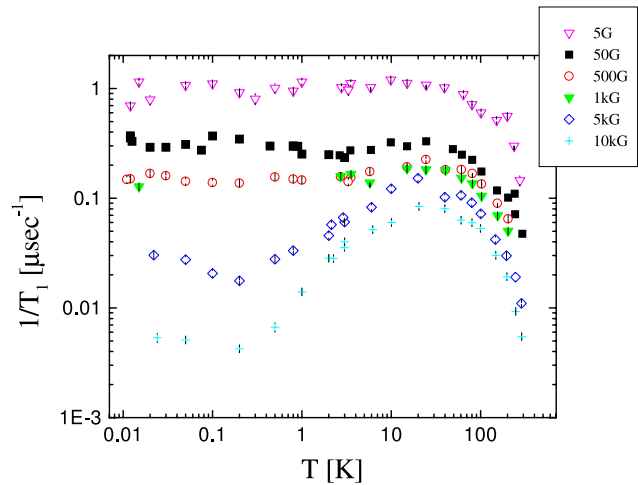


Fig. 165. The spin lattice relaxation rate as a function of temperature for different values of external magnetic field.

Experiment 960

Hydrogen (Mu) defects in II-VI chalcogenides

(*R.L. Lichti, Texas Tech; J.M. Gil, Coimbra*)

Zn chalcogenides

The basic plan of this run was to follow the behaviour of the normal muonium line in ZnSe as a function of temperature (as done in 2002 with ZnS) with the high-frequency spectrometer HiTime in M15. We used commercially available ZnSe single crystals from Crystec and Alpha-Aesar.

The Crystec sample was measured with the (100) direction parallel to the incoming muon beam and to the applied magnetic field. At 3.4 K and a field of 7 T, two lines are clearly visible at about 679 MHz and 763 MHz, as shown in the Fourier transform of Fig. 166. No significant diamagnetic amplitude is seen. Both lines are identified by their field dependence as the ν_{12} precession frequency of Mu^0 . This is a surprising result, as only one muonium state was previously known, with $A_{\text{HF}} = 3456.7$ MHz corresponding to the observed 763 MHz line (Mu_{I}). The much broader second line at 679 MHz (Mu_{II}) may either correspond to a novel state or to anisotropy of the known Mu^0 centre. Further experiments with differently oriented samples should clarify this aspect.

The amplitudes of these lines are approximately two-to-one in proportion, with the larger spectral weight in the broader Mu_{II} line. The amplitude and relaxation dependence on temperature up to the disappearance of these lines at about 50 K are shown in Figs. 167 and 168. The Mu_{II} relaxation rate is two orders of magnitude larger than that of Mu_{I} at the lowest temperatures. Both rate constants increase to the resolution limit as the amplitudes decrease.

Data for a second crystalline ZnSe sample, obtained from Alpha-Aesar, confirms two paramagnetic lines

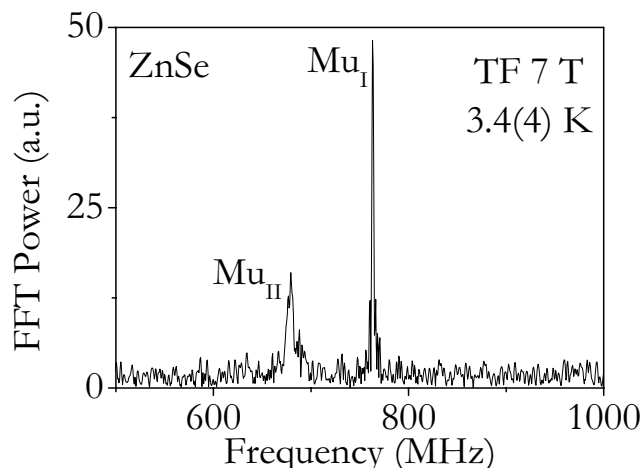


Fig. 166. Fourier transform of precession data for the ZnSe Crystec sample shows two paramagnetic lines, Mu_{I} and Mu_{II} , at low temperatures.

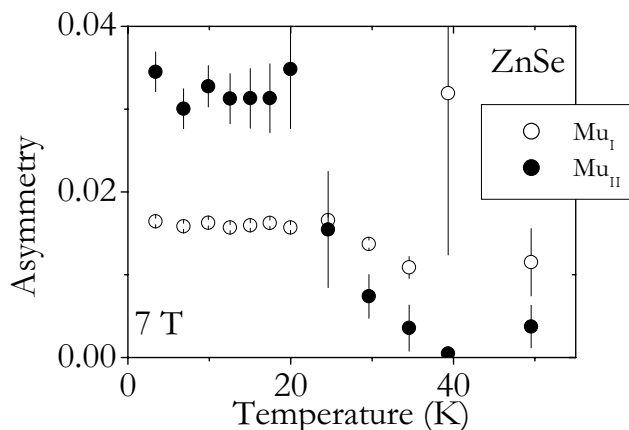


Fig. 167. Temperature dependent amplitudes of the paramagnetic lines observed for the ZnSe Crystec sample.

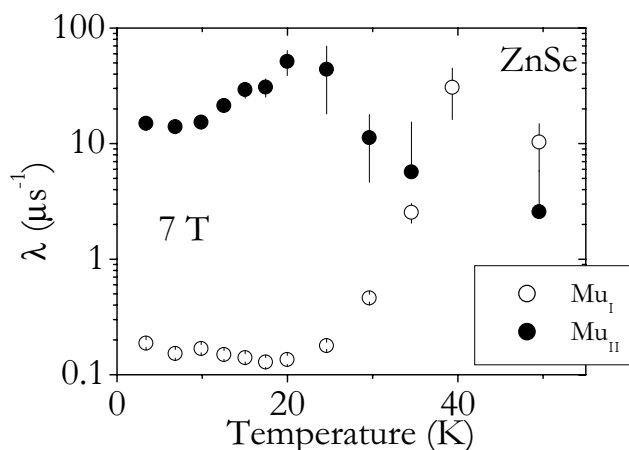


Fig. 168. Temperature dependent relaxation rates of the paramagnetic lines observed for the ZnSe Crystec sample.

with very similar amplitudes and relaxation rates at 3 K when compared to results from the Crystec sample. However, a crude temperature scan indicates persistence of the Mu_{I} line to much higher temperatures, whilst the Mu_{II} line seems to disappear at about the same temperature range in both samples. More detailed temperature dependences for the second sample deserve special attention in the near future. The sample related differences and different temperature dependences for the two lines seem to indicate two separate Mu^0 centres.

If we consider isotropic Mu^0 centres, a possible interpretation for the two states is that they would be located in the inequivalent tetrahedral cage sites of the zincblende structure. The hyperfine interactions obtained in this experiment match well with those calculated by Van de Walle and Blöchl [Phys. Rev. **B47**, 4244 (1993)], identifying Mu_{I} as located in the Zn cation cage and Mu_{II} in the Se anion cage.

CdTe

The case of CdTe is particularly interesting among the II-VIs in that both shallow and deep Mu^0 centres are apparently formed. The shallow Mu centre is visible at low temperatures in both n - and p -type materials with a low concentration of active native defects, and ionizes with an energy characteristic of a shallow-donor. The deep centre is inferred from a missing fraction and decoupling curves, but no precession signals are seen in transverse fields. In n -type samples, the diamagnetic fraction is involved in a dynamic process at temperatures above 150 K, revealed in low transverse fields by a decrease of its amplitude, large frequency and phase shifts, and an increase in the Lorentzian relaxation rate. This might indicate involvement of the deep centre in charge-exchange interactions with conduction electrons.

Measurements of T_1 relaxation as a function of longitudinal field and temperature are a way of extracting information on exchange rates and also of confirming the hyperfine interaction values of deep Mu^0 centres. One n -type undoped CdTe single crystal was measured in longitudinal fields with Helios in M20. Figure 169 shows the $1/T_1$ relaxation rates obtained as a function of temperature for a fixed low longitudinal field of 102 G.

Field scans were performed at the fixed temperatures of 220 K, 250 K and 265 K, as shown in Fig. 170. Although the decrease of the relaxation rate above 1 kG reveals the presence of a Mu^0 with a large hyperfine interaction, thus implying that a deep-level Mu^0 centre is the relaxing state, the slope of these curves does not have the B^{-2} dependence expected for a simple charge-exchange process involving an isotropic Mu^0 centre. We speculate that the processes responsible for the vanishing of the Mu^0 fraction in transverse fields, presumably a spin interaction during the final stages of thermalization of the implanted muon, might still play a role in this new situation.

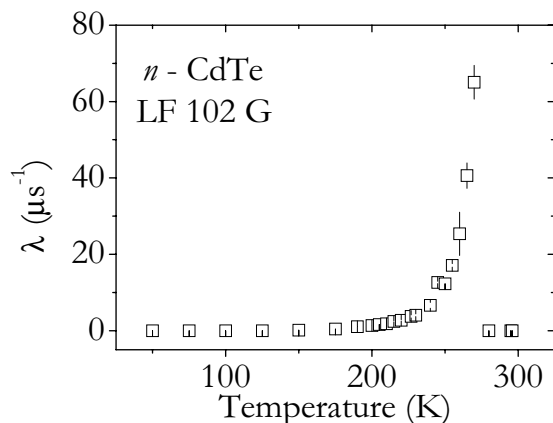


Fig. 169. Temperature variation of the relaxation rate at a fixed longitudinal field of 102 G, obtained for n -CdTe.

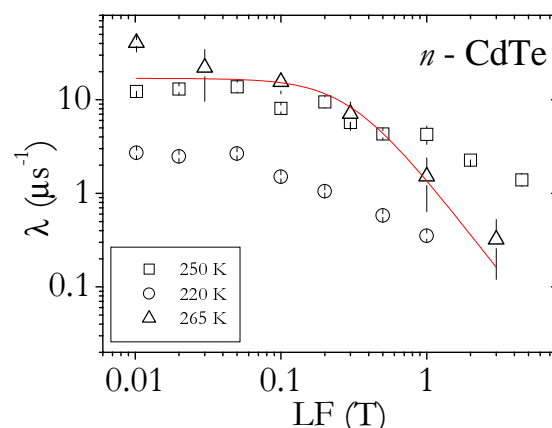


Fig. 170. Field variation of $1/T_1$ relaxation rates for n -CdTe, measured at a few constant temperatures.

Experiment 965

Investigation of spin dynamics in the new dipolar spin ice $\text{Ho}_2\text{Ru}_2\text{O}_7$

(C.R. Wiebe, Columbia/McMaster; G.M. Luke, McMaster; Y.J. Uemura, Columbia)

Frustration, a condition which describes the inability of a system to satisfy all of its individual interactions simultaneously, has become an important concept in the realm of condensed matter physics, being applicable to a wide range of phenomena such as high- T_c superconductors, liquid crystal phase transitions, and protein folding. A renewed interest in geometrically frustrated magnets has resulted from this general interest in frustration and the discovery of new magnetic ground states. One of these new states is the spin ice, which occurs on the pyrochlore lattice of corner sharing tetrahedra with weak ferromagnetic coupling between rare-earth ions subject to strong axial crystal fields. In particular, the $\langle 111 \rangle$ anisotropy of these sites promotes a “two-in, two-out” low temperature spin arrangement upon each tetrahedron, which is stabilized by dipolar interactions. The resulting ground state has a macroscopic entropy associated with the many ways that each tetrahedron can satisfy this condition independently of the other tetrahedra. The short-ranged order of this system maps onto the problem of proton ordering in the freezing of liquid water to ice. Pauling first realized the significance of the specific heat anomaly at the ice transition temperature as being due to the disorder at each oxygen site. An excellent agreement has been found between the spin ice model and physical properties including magnetization, specific heat, and neutron scattering experiments of the three spin ices, $\text{Dy}_2\text{Ti}_2\text{O}_7$, $\text{Ho}_2\text{Ti}_2\text{O}_7$ and $\text{Ho}_2\text{Sn}_2\text{O}_7$.

Recently, a new spin ice candidate has been discovered – $\text{Ho}_2\text{Ru}_2\text{O}_7$. Whereas other spin ices of the formula $\text{A}_2\text{B}_2\text{O}_7$ only have one magnetic species on

the A site, in $\text{Ho}_2\text{Ru}_2\text{O}_7$ both A and B sites are magnetic: Ho^{3+} $J = 8$ spins and Ru^{4+} $S = 1$ spins. Previous studies on the closely related pyrochlores in the series $\text{R}_2\text{Ru}_2\text{O}_7$ ($\text{R} = \text{Y}, \text{Nd}$) have revealed that the Ru^{4+} moments order at higher temperatures ($T \sim 100$ K). $\text{Ho}_2\text{Ru}_2\text{O}_7$ shows an anomaly in the magnetic susceptibility which agrees with these findings and suggests that the Ru^{4+} moments order at ~ 95 K. This claim was recently verified by neutron scattering measurements, which show very weak magnetic Bragg peaks forming.

The goal of our μSR experiments was to investigate how the Ru ordering influences the formation of the spin ice state at low temperatures. Zero-field (ZF) and longitudinal field (LF) measurements were completed on sintered powder samples of $\text{Ho}_2\text{Ru}_2\text{O}_7$. At ~ 95 K, there is no precession signal due to the paramagnetic Ho spins, which are much larger than the ordered Ru spins. However, we do observe a significant slowing down of spin fluctuations in the vicinity of T_N . The relaxation rate, obtained from fits to exponential relaxation, shows a dramatic rise at the transition (see Fig. 171). As well, the LF-spectra demonstrate a change in the spin dynamics below the transition at ~ 95 K (see Fig. 172). Recent neutron scattering measurements have shown that the Ho spins form spin clusters below ~ 95 K, which grow in size as the temperature is decreased. We see evidence for this with the change in spin dynamics in this temperature range.

Subsequent measurements were made at the Ho ordering temperature, where the ZF- μSR spectra show a highly damped response from the large ordered Ho moments. It is difficult to extract information as the relaxation rates move outside the window covered by conventional μSR .

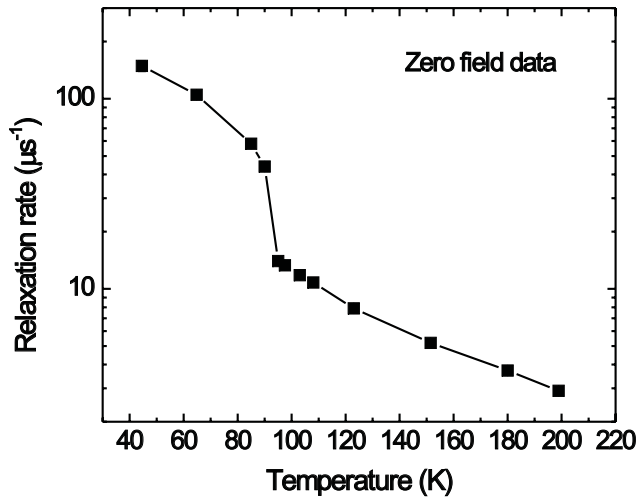


Fig. 171. Relaxation rates from ZF- μSR on $\text{Ho}_2\text{Ru}_2\text{O}_7$. Ru^{4+} spins are slowing down near the transition at ~ 95 K.

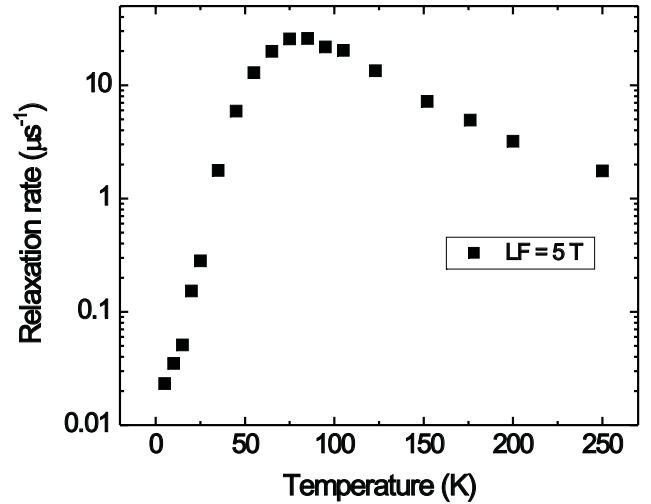


Fig. 172. LF- μSR on $\text{Ho}_2\text{Ru}_2\text{O}_7$ with $\text{LF} = 5$ T, indicating a change in spin dynamics in the region below the Ru ordering temperature (95 K), but above the Ho ordering at ~ 1 K. The Ho spins are believed to be forming spin clusters in this region.

Experiment 974

Unconventional superconductivity in $\text{Na}_x\text{CoO}_2 \cdot 1.3 \text{H}_2\text{O}$ and proximity to an ordered phase

(Y.J. Uemura, Columbia; C.R. Wiebe, Columbia/McMaster; G.M. Luke, McMaster)

Muon spin relaxation (μSR) measurements have been very effective in demonstrating unconventional superconductivity in high- T_c cuprate (HTSC) and organic superconductors. The absolute value of the measured penetration-depth λ established correlations between n_s/m^* (superconducting carrier density / effective mass) and T_c which, together with the pseudogap behaviour, suggest a formation of paired charge carriers occurring at a temperature significantly higher than the condensation temperature T_c . The temperature dependence of λ indicated d-wave pairing symmetry and line nodes in the energy gap. Zero-field μSR studies revealed and elucidated static magnetic order in parent compounds of HTSC.

To these superconductors based on strongly correlated electrons, the recent discovery of superconductivity in $\text{Na}_{0.35}\text{CoO}_2$ intercalated with $1.3 \text{H}_2\text{O}$ ($T_c = 4.2$ K) has added a unique compound which has highly 2-dimensional (2D) conducting planes of cobalt oxide in a triangular lattice structure with geometrical spin frustration. The original idea of resonating valence bonds was developed for this sublattice, but no superconducting system in this geometry has been known before the new cobalt oxide compound. Although extensive studies have been started, detailed characteristics of this system are yet to be demonstrated by conclusive experimental data sets.

Anhydrous Na_xCoO_2

We first describe zero-field (ZF) μSR studies of magnetic order in polycrystalline samples of non-superconducting anhydrous Na_xCoO_2 . Recent resistivity and susceptibility studies showed that the $x = 0.64$ system can be characterized as the “Curie-Weiss” metal, $x = 0.35$ as a “paramagnetic” metal, while $x = 0.5$ exhibits a transition from a high-temperature metal to low-temperature insulator at $T = 53$ K. In Fig. 173(a), we show the ZF- μSR time spectra of these systems. In the $x = 0.5$ system, the spectra above $T = 53$ K show slow relaxation without oscillation, i.e., a line shape expected for systems with nuclear dipolar fields without static magnetic order of Co moments. Below $T = 53$ K, a clear oscillation sets in, together with a rather fast damping. Below $T = 20$ – 25 K, we see two frequencies beating. Figure 173(b) shows the temperature dependence of these frequencies. The amplitude of the damping signal indicates that all the muons feel a strong static magnetic field below $T = 53$ K. The static magnetic order sets in at the onset of a metal-insulator transition, and the establishment of the second frequency takes place at $T = 20$ K, which roughly corresponds to the “kink” temperature in the resistivity shown in the inset. Although a conclusive picture requires neutron scattering studies, it seems that one of two interpenetrating Co spin networks acquires a long-range order below $T = 53$ K, followed by the other network establishing long-range order below 20 K. The spatial spin correlation should be antiferromagnetic (AF), since susceptibility shows no divergence at $T = 53$ K (evidence against ferromagnetism), and the damping of the $T = 25$ mK data is significantly slower than that of the Bessel function expected for the incommensurate spin-density-wave (ISDW) states (evidence against ISDW).

We also confirmed the absence of static magnetic order in anhydrous Na_xCoO_2 with $x = 0.35$ and 0.64 ,

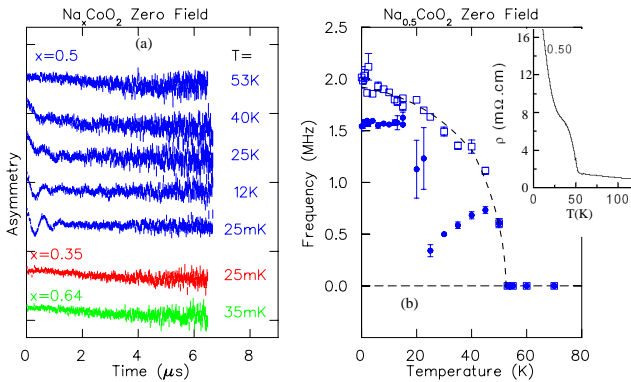


Fig. 173. (a) Muon spin relaxation time spectra observed in zero field in anhydrous Na_xCoO_2 with $x = 0.50$, 0.35 , and 0.64 . (b) The muon spin precession frequency observed in the $x = 0.5$ system, shown with resistivity in inset.

down to $T = 25$ – 35 mK, as shown in Fig. 173(a). Static antiferromagnetic order was reported for $x = 0.75$ – 0.9 by earlier μSR studies. Together, the present data establish a rather complicated evolution of the magnetic ground states from paramagnetic (PM) ($x = 0.35$) to AF (0.5) to PM (0.64) to AF (0.75) to ISDW (0.9), with increasing x . The ~ 2 MHz frequency in the $x = 0.5$ system is close to ~ 3 MHz in $x = 0.75$, suggesting that the ordered moment sizes in these systems are of comparable magnitudes. The existence of an insulating magnetic state in the vicinity of superconductivity resembles the case in the cuprates.

Superconducting $\text{Na}_x\text{CoO}_2 \cdot 1.3 \text{D}_2\text{O}$

We now focus on our results on powder samples of the superconducting phase, $\text{Na}_x\text{CoO}_2 \cdot 1.3 \text{D}_2\text{O}$. μSR data in transverse external fields (TF) reflect field broadening due to the flux vortex lattice in type-II superconductors, from which one can derive the magnetic field penetration depth λ . In Fig. 174, we compare the temperature dependence of $\sigma_{sc}(T) \propto \lambda^{-2}$ of $\text{Na}_{0.35}\text{CoO}_2 \cdot 1.3\text{D}_2\text{O}$ with various models, in a fit of 16 data points with $\sigma(T = 0)$ as a free parameter. The observed results clearly disagree with curves of the two-fluid model (normalized chi square NCS = 3.51) and s-wave BCS weak-coupling model (NCS = 1.75, Durbin-Watson value of a normalized residual error correlation DW = 1.11). Comparison with the scaled μSR results from YBCO yields NCS = 1.39 and DW = 1.59, showing a rather poor agreement yet in a statistically acceptable range. For a 5% confidence level, a model with NCS > 1.666 or DW < 1.1 or DW > 2.9 should be rejected, $1.1 < \text{DW} < 1.37$ or $2.63 < \text{DW} < 2.9$ is inconclusive, while $1.37 < \text{DW} < 2.63$ is comfortably acceptable.

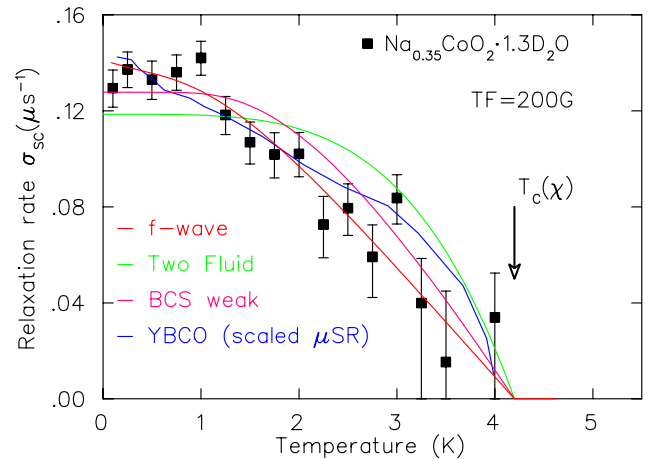


Fig. 174. Muon spin relaxation rate $\sigma_{sc}(T)$ due to superconductivity in $\text{Na}_{0.35}\text{CoO}_2 \cdot 1.3\text{D}_2\text{O}$, with $\text{TF} = 200$ G applied perpendicular to the aligned conducting planes, obtained by quadratic subtraction of $\sigma_{sc}^2 = \sigma_{exp}^2 - \sigma_n^2$. The results are compared with fits to several models and the scaled plot of μSR results on $\text{YBa}_2\text{Cu}_3\text{O}_{6.95}$ (YBCO).

For the cobalt oxide superconductors, several authors proposed f-wave models, which have a particular matching with the symmetry of triangular lattice. In Fig. 174, we also show a theoretical curve for an f-wave pairing, obtained by using a tight-binding fit of the LDA band calculation and by assuming a separable effective interaction supporting a simple f-wave order parameter. In the present system, there is a large Fermi surface around the Γ point as well as six small hole-pockets near the K points. The line in Fig. 174 represents a case where nodes of f-wave symmetry exist only on the large Fermi surface and not on the six hole-pockets, while the order parameter on each Fermi surface has the same maximum value. This f-wave model gives a good agreement with the observed data with $NCS = 1.19$ and $DW = 2.34$.

These results rule out a fully isotropic energy gap. Before concluding a particular pairing symmetry, however, one has to test various other models with and without the possible effect of impurities.

The penetration depth λ is related to the superconducting carrier density n_s divided by the effective mass m^* as $\sigma(T) \propto \lambda^{-2} \propto [4\pi n_s e^2 / m^* c^2] [1/(1+\xi/l)]$, where ξ is the coherence length and l denotes the mean free path. At this moment, it is difficult to prove the clean limit situation $\xi \ll l$ for the cobalt oxide superconductor, due to the lack of high-quality superconducting single crystals necessary to estimate the in-plane values of ξ and l . Derivation of the absolute values of λ and n_s/m^* is subject to modelling of flux vortex lattice line shapes, observed functional forms of field distribution, and angular averaging in the polycrystal samples. Based on the results of μ SR measurements on *c*-axis aligned YBCO and numerical works, we have adopted the conversion factor for polycrystal to aligned samples $\sigma_{\text{aligned}} \sim 1.4\sigma_{\text{poly}}$ to account for the effect of applying the TF perpendicular to the conducting planes of highly 2D superconductors. For σ to λ conversion $\lambda = A/\sqrt{\sigma}$, we have adopted a factor $A = 2,700 [\text{\AA}(\mu\text{s})^{1/2}]$ for the Gaussian width σ . With these conversion factors, the values of λ_{ab} of polycrystalline samples of underdoped YBCO with $T_c \sim 60$ K agree well with the value obtained using a single crystal specimen with comparable T_c in a more accurate lineshape analysis. The above factor A gives $\lambda = 7,200 \text{ \AA}$ for the in-plane penetration depth of the cobalt oxide system at $T \rightarrow 0$.

If we assume the charge carrier density to be equal to the Na concentration, we obtain the in-plane effective mass of the cobalt-oxide superconductor to be about 100 times the bare electron mass m_e . The heavy mass can be expected for strongly correlated carriers in a triangular lattice. The high effective mass is consistent with the electronic specific heat $C/T \sim 12$

[mJ/mole K²] of the superconducting cobalt oxide just above T_c . This value can be compared to ~ 2 [mJ/mole K²] of YBa₂Cu₃O₇. After normalizing the values to a unit sheet area of conducting planes, C/T for the cobalt oxide becomes about 25 times larger than that for YBCO. In the non-interacting 2D Fermi gas, C/T is proportional to m^* but independent of carrier density. Thus, within this approximation, we expect m^* of cobalt oxide to be 25 times that of the cuprates.

In conclusion, we have shown that the cobalt oxide superconductors have an anisotropic energy gap and a heavy effective mass $m^* \sim 100 m_e$. We have also established the existence of an antiferromagnetic insulating compound in the vicinity of the superconducting cobalt-oxide system without magnetic order, which suggests the possible involvement of magnetism in the superconducting mechanism.

Experiment 975 Magnetism and superconductivity in Na_xCoO₂·yH₂O and related cobalt oxides (W. Higemoto, R. Kadono, KEK-IMSS)

Recent discovery of superconductivity in a novel cobalt oxide, Na_xCoO₂·yH₂O ($x = 0.35, y = 1.3$) with the transition temperature $T_c \sim 4.5$ K, is attracting much interest [Takada *et al.*, Nature **422**, 53 (2003)]. The compound has a lamellar structure consisting of CoO₂, Na and H₂O bi-layers, where the two-dimensional (2D) CoO₂ layers are separated by thick insulating Na or H₂O layers. This structure is similar to high- T_c cuprate superconductors (HTSCs) in the sense that they also have a layered structure of 2D-CuO₂ sheets separated by insulating layers. It is well established that Cu²⁺ ($S = 1/2$) atoms on a square lattice exhibit antiferromagnetic (AF) ordering in the parent compounds of HTSCs, where the superconductivity occurs when the AF state is suppressed by carrier doping. On the other hand, Co atoms form a 2D triangular lattice on the CoO₂ layers, where a strong magnetic frustration is anticipated. Thus, while Na_{0.35}CoO₂·1.3H₂O may be viewed as an electron doped Mott insulator for a low-spin Co⁴⁺ ($S = 1/2$) with an electron doping $x = 35\%$, the electronic state may be considerably different from cuprates.

We conducted ZF- and HTF- μ SR measurements on the superconducting cobalt oxide and its deuterated specimen down to 2 K. We also made additional measurements on Na_{0.35}CoO₂·0.7H₂O with H₂O monolayers as a reference compound showing no superconductivity. The ground state property was examined by ZF- μ SR at KEK-MSL, while information on the superconducting pair correlation was investigated by the muon Knight shift deduced from HTF- μ SR at TRIUMF M15. Powder specimens of Na_{0.35}CoO₂·1.3H₂O

including a deuterated one ($D_2O \simeq 75\%$) were synthesized as described in Takada *et al.* [*ibid.*]. Each specimen was characterized by measuring magnetic susceptibility prior to μ SR measurement. For high field measurements, the powder specimen was secured with Apiezon-N grease to prevent an alignment of fine crystals in the specimen by strong field.

It turned out that the ZF- μ SR time spectra below 10 K can be well reproduced by the Kubo-Toyabe relaxation function. The lineshape exhibits the least dependence on temperature over the temperature range through T_c . A large difference in the nuclear dipolar width (Δ) between hydrate and deuterate specimens indicates that muons occupy a site close to the water molecule. By comparing Δ between those two specimens together with calculated mapping of Δ , the muon site is identified near (0.2, 0.25, 0.12). Since this site has a lower symmetry, it is unlikely that the internal fields from cobalt oxides happened to be cancelled. Thus, we conclude that there is no spontaneous internal magnetic field associated with the occurrence of superconductivity nor any symptom of magnetism down to 2 K.

The magnetic penetration depth (λ) in the hydrate specimen is deduced to be about 5000 Å from TF- μ SR data at lower fields. This long λ does not allow us to discuss the temperature/magnetic field dependence of λ in detail; the corresponding relaxation rate due to the flux line lattice (FLL) formation ($\sigma \simeq 0.1 \mu s^{-1}$) is too small to be determined experimentally with enough precision. On the other hand, the diamagnetism for such a long λ can be negligible at high fields, and thereby we can study the muon Knight shift without much ambiguity due to the FLL formation.

In general, the muon Knight shift $K(T)$ is expressed as $K(T) = K_s(T) + K_{orb}$. Here, K_s and K_{orb} are the spin and orbital component of the Knight shift, and only $K_s(T)$ is temperature dependent. Then, as shown in Fig. 175, $K_s(T)$ is determined by the slope of the muon Knight shift versus magnetic susceptibility (K - χ plot) irrespective of K_{orb} (which is set to zero in this analysis). Figure 176 shows the temperature dependence of $K_s(T)$ (at 60 kOe) and uniform susceptibility (at 10 kOe) in the randomly oriented sample of $Na_{0.35}CoO_2 \cdot 1.3H_2O$. The muon Knight shift decreases with decreasing temperature below 100 K and levels off below 10 K. Above 10 K, $K_s(T)$ is proportional to the uniform susceptibility, which clearly indicates that the upturn of the $\chi(T)$ below ~ 100 K is due to some intrinsic origin. The spin part of the muon Knight shift is expressed as $K_s = A_{hf}\chi$, where A_{hf} is the hyperfine coupling constant. From the above relation, A_{hf} is estimated to be ~ -134 Oe/ μ_B . It should be noted that

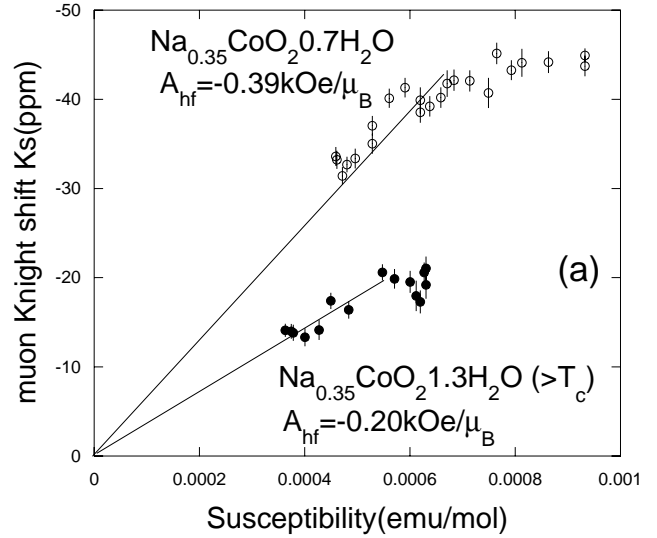


Fig. 175. The muon Knight shift (at 60 kOe) versus susceptibility plot in $Na_{0.35}CoO_2 \cdot yH_2O$; it exhibits superconductivity for $y = 1.3$ while it remains normal for $y = 0.7$.

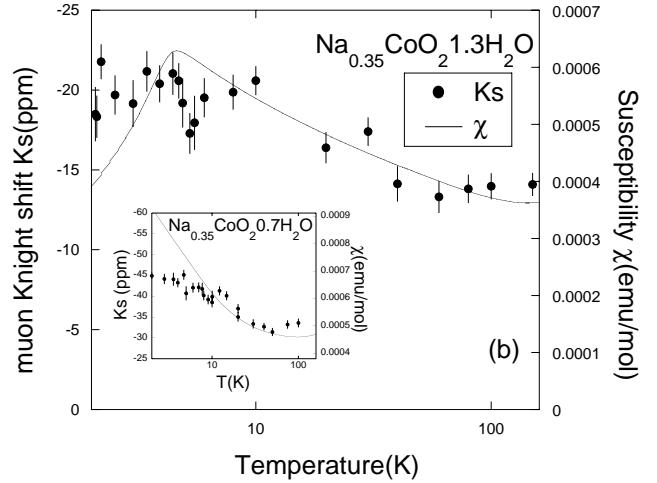


Fig. 176. Temperature dependence of the spin part of the muon Knight shift K_s (filled dot) and susceptibility (solid line). Susceptibility was measured at 10 kOe.

the anisotropic term of the Knight shift, or so called powder pattern, is not seen in the spectra. This implies that the anisotropy of the Knight shift is much smaller than the present resolution. In the case of s -wave pairing superconductivity, K_s decreases to zero with decreasing temperature following the Yoshida function. However, as shown in the inset of Fig. 176, the muon Knight shift does not show any appreciable reduction below T_c .

Since the observed muon Knight shift is negative, there remains a possibility that the reduction of K_s below T_c may be cancelled by the diamagnetic shift upon the formation of FLL. We estimated the magnitude of such a diamagnetic shift taking account of the effects of dense overlap of vortices and the Doppler

shift; the latter is present when the superconducting gap has nodes, leading to further enhancement of λ . This is reasonable considering the recent NMR measurements suggesting line nodes in this compound. Our simulation yielded that $\lambda \simeq 12 \mu\text{m}$ at 60 kOe where the

associated diamagnetic shift by the FLL formation is less than 2.8 ppm, which is too small to cancel out the predicted effect due to spin singlet superconductivity. Thus, we conclude that the result in Fig. 176 is mostly attributed to K_s .